UNIVERSITY OF GHANA

PHOTOCATALYTIC DEGRADATION OF ORGANIC DYES USING ZINC OXIDE NANOPARTICLES.

BY

ASIEDU THEOPHILUS

(10391669)

DEPARTMENT OF MATERIALS SCIENCE AND ENGINEERING.

UNIVERSITY OF GHANA

This Thesis is submitted to the University of Ghana, in partial fulfilment of requirement for the award of Master of Philosophy in Materials Science and Engineering Degree.

2018.

UNIVERSITY OF GHANA

PHOTOCATALYTIC DEGRADATION OF ORGANIC DYES USING ZINC OXIDE NANOPARTICLES.

BY

ASIEDU THEOPHILUS

(10391669)

DEPARTMENT OF MATERIALS SCIENCE AND ENGINEERING.

UNIVERSITY OF GHANA

This Thesis is submitted to the University of Ghana, in partial fulfilment of requirement for the award of Master of Philosophy in Materials Science and Engineering Degree.

JULY, 2018.

DECLARATIONS

Candidate's Declaration.

I hereby declare that this project report which is the result of my own original research was prepared in accordance with the University of Ghana's academic regulations and that no part of it has been presented for another degree in this University or elsewhere.

Candidate's Name: **Asiedu Theophilus (10391669)**

Signature: …… Date: …….

Supervisors' Declaration

I hereby declare that the preparation and presentation of the project report were supervised in accordance with the guidelines on supervision of project reports laid down by the University of Ghana.

Supervisor's name: **Dr. David Dodoo-Arhin**, (University of Ghana)

Signature: …… Date: ……

Co-Supervisor's name: **Prof. Julius M. Mwabora**, (University of Nairobi, Kenya)

Signature: …… Date: ……

Head of Department's Declaration.

I hereby declare that the project report has been prepared, supervised and accepted in accordance with the guidelines on project works laid down by the University of Ghana.

Head of Department's Name: **Dr. Lucas Damoah**

Signature: ……. Date: ……..

ABSTRACT

Nanocrystalline zinc oxide particles were synthesized via sol-gel method using zinc acetate as precursor. Calcination temperature was varied to determine its effect on particle size. The resultant samples were subjected to X-ray Diffraction (XRD), Fourier Transform Infra-Red (FTIR), UV-visible and Scanning Electron Microscopy (SEM) characterization techniques. X-ray diffraction results showed nanocrystalline wurtzite ZnO particles with crystallite size ranging from 16 nm to 30 nm respectively. FTIR detected bands below 1000 cm^{-1} representing Zn and Zn-O bonds, UV-vis showed absorption of ZnO particles in the ultraviolet range. Band gap energy of synthesized zinc oxide nanoparticles decreased with increasing calcination temperature and increasing crystallite size. Micrographs from SEM showed rice-like microstructure morphology of ZnO nanoparticles.

The usage of ZnO nanoparticles as a photocatalyst was also explored in the degradation of Rhodamine B and Methylene Blue using UV-light with particular attention of the effect of particle size and catalyst load on the degradation efficiency of the respective dyes. Reusability of ZnO nanoparticles for photocatalytic degradation was also explored in this work.

Results from photocatalytic degradation of Rhodamine B and Methylene Blue showed that nanoparticles calcined at 400 ℃ which has crystallite size of 16 nm had the highest degradation efficiency on both dyes with 93.5 % and 95.4 % degradation on Rhodamine B and Methylene Blue respectively. Results also showed that 0.2 g catalyst load exhibited the highest degradation efficiency with 95.41 % and 97.97 % degradation of Rhodamine B and Methylene Blue dyes respectively. Reusability of ZnO nanoparticles for photocatalytic degradation of RhB and MB over four different cycles showed a decrease in degradation efficiency from one cycle to another.

ACKNOWLEDGEMENT

My sincere thanks and profound gratitude to Almighty God for His goodness and mercy during the course of my university education as an MPHIL student and also for a successful execution of my research work. My utmost gratitude and respect to my research advisor and supervisor, Dr. David Dodoo-Arhin, for his unwavering assistance and contribution to this research work and also to Professor Julius M. Mwabora of University of Nairobi. Also my profound gratitude to Mrs. Gloria Pokuaa Manu and Mrs. Grace Kakari of Materials Science Laboratory and also to the laboratory technicians of University of Ghana Biotech Centre for allowing me perform part of the experimental work in their laboratories. Also to the staff of University of Ghana Ecological Laboratory of the Department of Geography for their time and support. To the Head of Department of Materials Science and Engineering and the entire faculty of Materials Science and Engineering Department especially Dr. Emmanuel Nyankson, I say a big thank you for their time and support. Finally, my sincere appreciation to my parents, my colleagues and everyone who helped me throughout this project. God bless you all.

DEDICATION

This work is dedicated to myself and my family for the support they have given me so far in my university education. I also dedicate it to Mr. Samuel Buabeng for His kind support over the years.

TABLE OF CONTENT

LIST OF FIGURES

LIST OF TABLES

LIST OF ACRONYMS AND ABREVIATIONS

Z_400	Zinc Oxide Nanoparticles calcined at 400 ºC
Z_500	Zinc Oxide Nanoparticles calcined at 500 ºC
Z_600	Zinc Oxide Nanoparticles calcined at 600 ºC
XRD	X-Ray Diffraction
SEM	Scanning Electron Microscopy
FTIR	Fourier Transform Infra-Red
UV	Ultra-Violet
RhB	Rhodamine B
MB	Methylene Blue
FWHM	Full Width at Half Maximum
WPPM	Whole Powder Pattern Modelling

CHAPTER ONE

1.0. Introduction

Improper disposal of residual dyes and dye effluent into water bodies by some industries and local textile manufacturers has become a major contributor to the pollution of water bodies in recent times [1]. This poses enough threat to humans, livestock and the aquatic ecosystem since these dyes are carcinogenic and have poor biodegradability [2]. Particular attention has been paid to organic dyes as major environmental pollutants due to their non-biodegradability and harmful effects on humans owing to their high potential of been carcinogenic [3], [4]. Moreover, they have deteriorating effect on the nature and quality of water, and also impede the permeation of sunlight at the detriment of photosynthetic aquatic plants. For instance, traces of an organic dye such as Methylene blue (MB) in water, can result in ailments such as abdominal disorders, irritations and other related disorders such as anemia as result of hemolysis [4]. However, the use this dye is very vital to making textile products in the industry especially in dying fabrics [5]. An annual estimation on the use and production of dyes and pigments worldwide reveals that more than 10,000 dyes and pigments are used and 7×10^5 tons are produced synthetically [6] which is an indication that the use of these dyes cannot be avoided since they form an integral part of industrial operations especially in the textile and paper industries. Therefore, there is the need to inhibit the harmful effects of these dyes on the ecosystem. Over the years, work has been done to reclaim dye polluted water using some water treatment techniques such as adsorption, coagulation and membrane separation [7]. However, these techniques only enhanced the conversion of the pollutants in the water into the solid phase resulting in the generation of secondary pollutants which may have adverse effects on the ecosystem [8]. Therefore, a more effective and safe method of removing these dyes without the generation of secondary harmful products is needed.

In view of this, degradation of dyes dissolved in water via photocatalysis using semiconductor nanoparticles as photocatalyst has been explored in recent times for the removal and reclamation of dye polluted water bodies and has gained much interest in this regard [9]. The technique is highly beneficial and safe as it is suitable for purifying water that has some concentration of dye contaminants without yielding toxic intermediate products in most cases [10]. These semiconductor nanoparticles in the presence of light at a specific wavelength can generate electron-hole pairs [11] which undergo series of oxidation and reduction reactions to produce hydroxyl groups as the main oxidizing agent to breakdown the organic components of the dye into green products [12]. A number of photocatalysts explored over the years include titanium dioxide (TiO_2), copper (II) oxide (CuO), zinc oxide (ZnO) and many others [13]. Amongst these catalysts, titanium dioxide has been widely used and explored in several studies owing to its photoactivity and ability to oxidize these dyes into green products [14] amidst some challenges such as low quantum effect and surface area [15]. However, zinc oxide in the light of the challenges posed by titanium dioxide, has also gained much attention as a favourable alternative material for photocatalytic degradation of dye polluted water as it exhibits good photo activity and photo luminescence properties [16] with relatively high surface area and quantum yield compared to titanium dioxide [17]. It also has a high tendency of exhibiting high reaction and mineralization rates leading to the generation of hydroxyl ions which are the main oxidizing units [18].

Zinc Oxide is a heterogeneous n-type semiconductor material having a wide direct band gap of about 3.37 eV and an exciton binding energy of about 60 meV [19]. With respect to its band gap energy, zinc oxide exhibits ultraviolet light (UV) absorption at room temperature and poor response to visible light in the electromagnetic spectrum. This restricts the intrinsic semiconductor to be used actively as a photocatalyst under a visible light source [4]. However, the bandgap of

zinc oxide can be modified through doping it p-type to increase its absorption spectrum into the visible light region [20]. Moreover, achieving p-type zinc oxide poses some challenges as the semiconductor exhibits n-type conductivity with the presence of vacancies and zinc interstitials which constitute native point defects in the material [21]. Applications of ZnO span through various areas including catalysis, optoelectronics, gas and bio-sensors, active filler for rubber and plastic, UV absorbing agent in cosmetics and many others [22]. ZnO nanoparticles and powders with different surface morphologies and nanostructured geometries can be synthesized using simpler synthesis techniques including sol-gel, hydrothermal, precipitation, micro emulsion synthesis, mechanochemical and combustion techniques [5], [23].

In this study, synthesis of zinc oxide nanoparticles was carried out using the sol gel technique. Sol-gel technique is used because it is simple, has the ability to control the morphology of nanoparticles and also favourable for synthesizing nanoparticles with good optical properties for various applications. The photoactivity of zinc oxide nanoparticles at different calcination temperatures was explored by using it as a catalyst for the photo-induced degradation of Methylene Blue and Rhodamine B under UV light. Finally, the rate of degradation with increasing catalyst load was analyzed using methylene blue and Rhodamine B and the reusability of catalyst.

1.1 Problem Statement.

Water bodies are usually polluted with dye effluents from industries such as textile and paper industries, and domestic operators of tan and dye in our society. A report by starrfmonline.com on Saturday 7 October ,2017 captioned “Shock as Nsukwa river turns red” revealed that, dye disposal into the river may be the cause of its colour change based on police preliminary investigations. This is a typical incidence of improper dye disposal in our environment. These dyes, result into severe pollution of water bodies since they are not self – degradable or bio – degradable. They

pose a lot of problems such as destruction of aquatic life, ailments and carcinogenic effects to both humans and animals. Several reclamation methods such as coagulation to recover dye polluted water do not suitably remove dye concentrates from water and therefore photocatalytic degradation of dyes will be explored in the study for the removal of dye concentrates from water.

1.2 Hypothesis.

Photocatalytic degradation of organic dyes is aided by the presence of a light at a particular wavelength and the presence of a photocatalyst.

1.3 Aims and Objectives.

i. To synthesize zinc oxide nanoparticles via sol-gel technique.
ii. To explore the degradation of dyes in water using zinc oxide nanoparticles via photocatalytic reaction and the of crystallite size effect on the rate of degradation.
iii. To explore the possible effect of different catalyst load on the degradation rate.
iv. To explore the reusability of zinc oxide nanoparticles as photocatalyst.

CHAPTER TWO

2.0. Literature Review

2.1 Semiconductor Nanomaterials.

Nanotechnology and its applications have over the years made significant contributions and progress to many fields ranging from electronics, energy, health and environmental sciences in the world. This explains why nanotechnology and nanosciences have gained much interest, even in the 21st century [24]. Nanomaterials and nanostructures appear to be very instrumental in materials science and engineering due to their enormous applications in nanotechnology. The research into of nanomaterials and nanostructures has introduced novelty in the principles and techniques needed to approach and investigate various problems, thereby contributing potentially to the resolution of several scientific problems in the world today [24].

Recently semiconductor nanomaterials preparation, characterization and application are explored by several researchers because the size of these materials give them different properties and enables them to be used for various applications [24], [25]. There have also been a number of applications for nanomaterials in recent years. This includes photovoltaics, biomaterials, diodes, laser technology, chemical and biosensors, superabsorbents and catalysts [22]. Examples of such semiconductor nanomaterials include Silicon, and other heterogeneous semiconductor materials such as Zinc Oxide, Titanium dioxide, Silicon-Germanium, Gallium-Arsenide, Aluminum Gallium Arsenide, Gallium Nitride, Zinc Selenide, Cadmium Selenide and many more [24]. Nanoparticle research is very significant to the miniaturization of most electrical and optical devices in the world today and this is one of the factors that has increased nanotechnology research [26].

2.2 Zinc Oxide and Its Properties.

ZnO is a heterogeneous semiconductor material which appears physically as a crystalline powder with a characteristic white colour. It occurs naturally as Zincite. Research studies on ZnO had been extensively done for several past decades as far back as the 1950's with some notable theoretical and characterization works on ZnO occurring in the 1960's [27]. Research on the preparation ZnO nanoparticles has been increasingly intensified over the years since it is found to be more desirable in a number of applications.

Zinc oxide has a distinctive physical and good chemical properties, that include high thermal stability, chemical stability, high electrochemical coupling coefficient, wide absorption spectrum of light and better photostability amongst many others. This combination of properties makes it multifunctional [28]. For instance, its wide band gap and high bond energy (60 meV) coupled with good thermal and mechanical stability contributes to its suitability for electronics and optoelectronics applications [29]. Also, ZnO owing to its piezoelectric and pyroelectric tendencies have been used extensively towards the research and production of biosensors, catalytic converters, energy generation devices and photocatalyst for several photocatalytic reactions [22], [30]. Nonetheless, it also has applications in the ceramic industry owing to its hardness, rigidity, high piezoelectric constant and the biomedical industry due to its biocompatibility, biodegradability and low toxicity [31]. Moreover the microstructure of the material can also be tailored in order to fetch certain desirable properties for specific applications [32]. A number of the variety of physical structures or morphologies of zinc oxide at the nanoscale includes one dimensional (such as needles, nanowires and nanorods), two-dimensional (such as nanopellets and nanosheet), and three dimensional structures (such as nanoflowers) [24]. This reveals that ZnO has a wide variety of physical morphologies which can suit different applications.

2.3 Crystal Structures of Zinc Oxide

The crystal structure of zinc oxide is categorized generally into two major forms, hexagonal wurtzite and cubic zinc blende. Both the zinc blende and the hexagonal wurtzite structures have coordination number four [28], [29].

2.3.1 Wurtzite Crystal Structure.

The wurtzite crystal structure is the thermodynamically stable crystal unit of zinc oxide. It exhibits better environmental stability than the zinc blende structure. This is because the wurtzite structure is identified with a characteristic high ionic interaction that exist between zinc and oxygen ions in the material. In general, the ionicity can be attributed to the c/a ratio of the crystal structure. A higher c/a ratio indicates a lower stacking fault energy, and a lower ionicity [33]. The stacking fault energy is related to the compressive or tensile strains coupled with imbalances in the interfacial chemistry of the material. Also the presence of a space group (P63mc space group) in the crystal contributes to no centre of inversion symmetry in the crystal. This effect leads to its piezoelectric properties [33]. Moreover, in the absence of external fields, strain-induced polarization occurs as a result of macroscopic polarization in the wurtzite structure [33]. Below (Figure 2.1) is the wurtzite crystal structure and unit cell of zinc oxide.

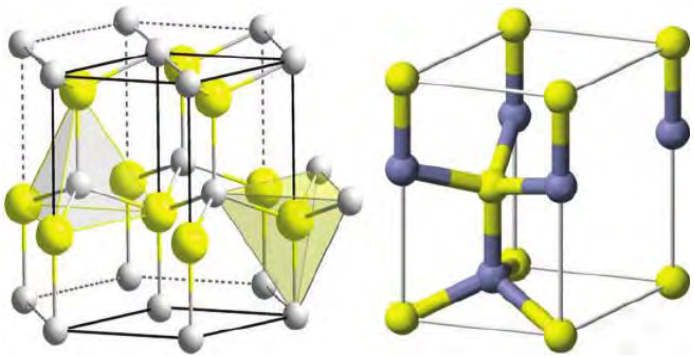

(a) **(b)**

Figure 2.1: (a) Wurtzite crystal structure (b) Unit cell of wurtzite structure of zinc oxide. [29]

2.3.2 Zinc Blende Crystal Structure

The zinc blende crystal structure of zinc oxide is metastable in nature owing to lower ionicity in the crystal compared to the wurtzite structure [33]. In effect, the Zinc blende crystal of the material is considered as covalent and it is suitable for several semiconductor applications [33]. The crystallographic symmetry underlying the zinc blend structure is higher and makes it potentially good for some device applications. This symmetry explains the piezoelectric polarization effect related with this structure as a result of the existing strain in the [001] directions [33]. Typically, the Zinc blende crystal unit unlike the wurtzite, is associated with complete and unique band dispersion of valence and conduction bands. This accounts for the possibility of getting the required band structure parameters for device modeling [33]. Below (Figure 2.2) is the unit cell structure of the Zinc blende crystal structure of zinc oxide.

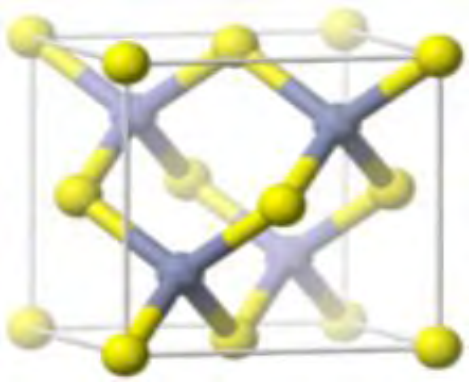

Figure 2.2: Unit cell of zinc blende crystal structure of ZnO [28].

2.4 Methods of Synthesis of Zinc Oxide Nanoparticles.

A number of techniques have been explored over the years for the synthesis of zinc oxide nanoparticles with desirable crystal structure, microstructure morphology and properties for

specific applications. Some of these synthesis techniques include Sol-gel [34], Solvothermal/Hydrothermal [35] and mechanochemical process [36].

2.4.1 Sol-Gel Technique.

Sol-gel technique is a considerably low temperature method which has been explored since the late 1800s [24]. In sol-gel technique, precursors prepared from inorganic substances are used to produce highly homogeneous powders, ceramics or glasses with high level of purity [37]. Processes involved in sol-gel include the formation of precursors by the hydrolysis of a metal alkoxide, condensation and polycondensation reactions to form a 'sol' and subsequently an aerogel. Basically, the sol-gel method involves phase transformation of a 'sol' into a gel. A 'sol' generally consists of chains of solids, globules or oligomers dispersed in a medium such as water or an organic solvent [24].

A gel is a continuous phase of solid mass obtained from the sol after aging [24]. It is usually having a higher viscosity than the sol. One significance of the sol-gel method over high temperature conventional methods is the ability to produce materials with high purity and different morphologies [34] amidst its low operational cost. This makes it a more favourable method than high temperature conventional techniques.

The sol-gel technique can be employed in the synthesis of wide range of materials to attain certain properties required for various applications such as photovoltaics, biosensors, catalyst amongst others [24]. It has the potential to retain the compositions of precursors used in the process to obtain a product of the same proportion. Knowledge about sol-gel technique has been applied across different research disciplines for the production of both thin films and bulk materials. Another advantage of this technique is the flexibility of the process in terms of the chemicals used as well as the ability to control kinetics of the process making it possible to achieve desired end

products and avoiding any alteration of the material produced [38]. Sol-gel synthesis of ZnO powder using zinc acetate dehydrate as precursor and oxalic acid was prepared by Benhebal *et al.* [38]. The XRD and SEM results of the prepared powder indicates a hexagonal wurtzite structure and a spherically shaped morphology respectively. Also BET results of the prepared powder also show that the material is less porous with a surface area value of 10.5 m^2/g [38].

2.4.2 Solvothermal /Hydrothermal Technique.

The solvothermal method is also a suitable method employed in many research works due to its potential use in producing a wide variety of micro and nanoparticles with unique physical morphologies and properties. In solvothermal process, a reaction in a closed system especially an autoclave is initiated in the presence of a solvent at a particular temperature and pressure [24]. The temperature in the closed system is usually kept above the boiling temperature of the solvent present and it is also dependent on the type of reaction involved.

The hydrothermal method is a solvothermal technique but involves the usage of water as the solvent. Organic solvents are not required for hydrothermal synthesis [27]. It also requires no further processing of the material such as calcination. The method is characterized by heating in an autoclave at a specific temperature and subsequently cooling to form crystals which are allowed to grow. Hydrothermal method is a low temperature method and also has a number of advantages such as the ability to produce materials of diverse shapes or morphology, high purity and high degree of crystallinity [39], [40]. An example of hydrothermal synthesis is that reported by Dem'Yanets *et al.* [40] in the synthesis of nanocrystalline zinc oxide using zinc acetate or a zinc salt and a hydroxide in a reaction to produce a $Zn(OH)_2 \cdot nH_2O$ precursor which undergoes heat treatment in an autoclave to produce a hexagonal crystals of zinc oxide with sizes ranging from 100 nm to 20 um. Hydrothermal method has attracted many studies towards its potential use in

both research and industrial applications. For instance, in mineral extraction it has been explored for leaching ores [24]. It has also been used for the possible purification of geological minerals [41] and synthesis of novel materials with specified morphologies [42]

2.4.3 Mechanochemical Process.

The mechanochemical synthesis technique is a solid state processing technique which involves milling of anhydrous starting materials at low temperatures using a ball mill or planetary mills [43]. Chemical transformations occur as a result the ball-particle impact [36], [44]. Milling is done using planetary mills and the reaction is performed in a ceramic or stainless steel vessel [36]. The particles are separated by a reaction medium also known as thinner. This is followed by calcination to obtain the final product. The method is appropriate for the mass production of nanoparticles and has low particle agglomeration tendencies. However, a major drawback of this method is the non-homogeneity of particles obtained and the tendency of impurities in the final product if there is a longer milling time. Particles of anhydrous materials mainly used as starting materials in this method are separated after milling with the application of NaCl which serves as a thinning material [21].

2.5 Photocatalysis.

Photocatalysis involves the use of light and a catalyst to perform some chemical reactions, for instance in the photodegradation of dye concentration in water. It remains a laudable approach especially in the reclamation of water containing organic pollutants [45]–[47]. In the process, organic pollutants are degraded via photo-induced oxidation reactions in the presence of a semiconductor photocatalyst [48]–[50]. This occurs when a semiconductor photocatalyst is illuminated with light whose photon energy is greater than that of the material's bandgap energy.

Excitation of electrons (e^-) occurs which results in the movement of electrons from the valence band into the conduction band leaving holes (h^+) in the valence band. In effect, electron-hole pairs are created which initiate series of photo-oxidative reactions. The holes undergo reactions with water to generate hydroxyl radicals (OH•) which are the main oxidants needed to degrade organic pollutants [51]. The excited electrons in the material's conduction band also undergo a reaction to reduce oxygen molecules dissolved in the liquid medium (water) into superoxide radicals [29].

Several semiconductor materials have been explored as photocatalysts for photocatalytic activities. Examples are TiO_2, ZnO, CuO, and WO_3 among others [24]. One factor that affects the use of a semiconductor as a photocatalyst is the bandgap energy. The bandgap energy reveals the limits of the absorption spectrum of the material. This is necessary because it shows the minimum photon energy needed to initiate photoreactions [29], [52], [53]. Among the several semiconductor photocatalysts, TiO_2 has over the years been explored the most in photocatalytic studies [54]. However, in recent times, ZnO has also received considerable attention as a potential photocatalyst and alternative to TiO_2 due to its band gap energy and other optical properties. Reports from other studies indicate that ZnO has higher electron-hole pair generation efficiency making it more photoactive compared to TiO_2. ZnO also has a large quantum size effect which makes it more suitable for photocatalytic activities [54]–[57].

2.5.1 Photocatalytic activity of Zinc Oxide Nanoparticles.

ZnO is more active as a photocatalyst in the UV region of the electromagnetic spectrum due to its band gap energy. The photocatalytic action of ZnO particles involves a number of steps. Reports by Herrmann et al [11] indicates that the photocatalytic activity of ZnO involves a number of steps which are outlined below:

1. Diffusion and adsorption pollutants onto the surface of ZnO.

2. Photo-induced redox reactions occurring on the surface of ZnO.

3. Desorption of resultant products.

ZnO particles are photo-induced to generate electron-hole pairs, as shown in equation (2.1) when illuminated with light with photon energy greater than the bandgap energy of ZnO.

$$ZnO + hv \rightarrow \left(e^{-}_{(CB)}\right) + \left(h^{+}_{(VB)}\right) \quad \text{..... (2.1)}$$

The electron-hole pairs generated by the photoreaction undergo redox reactions as shown in equations $(2.2 - 2.4)$ below. $The\ holes\ (h^{+}\ ions)$ oxidizes water to release hydroxide ions and subsequently oxidizes hydroxide ions at the surface of the particles into hydroxyl radicals (equation 2.2 and 2.3). Electrons, e– reduces oxygen into superoxide radical anions (equation 2.4) and subsequent reactions between superoxide radical anions and H^{+} ions generate hydroperoxyl compounds which combine to form hydrogen peroxide (equations 2.5 and 2.6) [61, 11].

$$\left(h^{+}_{(VB)}\right) + H_2O \rightarrow H^{+} + OH^{-} \quad \text{..... (2.3)}$$

$$\left(h^{+}_{(VB)}\right) + OH^{-} \rightarrow OH\cdot \quad \text{..... (2.3)}$$

$$\left(e^{-}_{(CB)}\right) + O_2 \rightarrow O_2{}^{\cdot -} \quad \text{..... (2.4)}$$

$$O_2{}^{-} + H^{+} \rightarrow HO_2\cdot \quad \text{..... (2.5)}$$

$$HO_2\cdot + HO_2\cdot \rightarrow H_2O_2 + O_2 \quad \text{..... (2.6)}$$

Further reaction between hydrogen peroxide and superoxide radicals results in the generation hydroxyl radicals as shown in equation (2.7). Also excess hydrogen peroxide is converted into hydroxyl radicals in the presence of light as shown in equation (2.8) below:

$$H_2O_2 + O_2{}^{\cdot -} \rightarrow OH\cdot + OH^{-} + O_2 \quad \text{..... (2.7)}$$

$$H_2O_2 + hv \rightarrow 2OH\cdot \quad \text{..... (2.8)}$$

The hydroxyl radicals released are the main oxidizing agents that break down complex organic pollutants adsorbed on the ZnO and convert them into intermediate products and subsequently into green products such as water and carbon dioxide as shown in equations (2.9 and 2.10) [58].

Organic pollutants + OH• → Intermediates…… (2.9)

Intermediates → $CO_2 + H_2O$ …….. (2.10)

The photocatalytic mechanism of zinc oxide nanoparticles is depicted in **Figure 2.3** below.

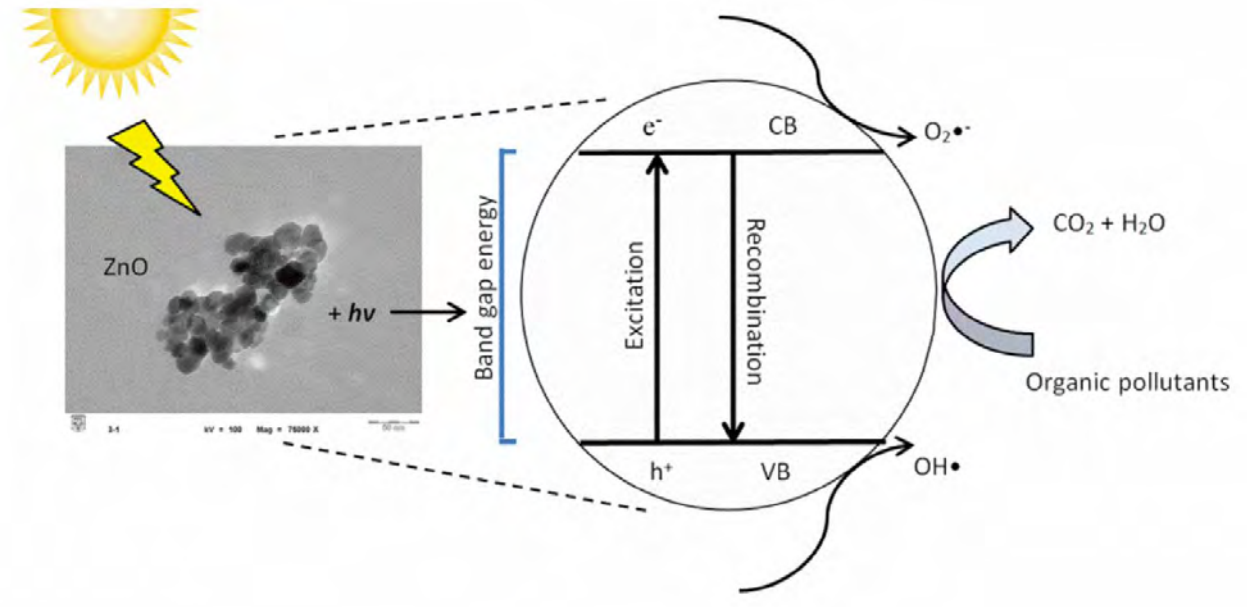

Figure 2.3: Photocatalytic action of ZnO in the degradation of dyes [59].

Although ZnO is a favourable semiconductor photocatalyst, it also has a few drawbacks that hinder its photocatalytic efficiency. One of these drawbacks is the tendency of recombination of photogenerated electrons and holes to occur which may hinder effective photoreactions to degrade organic pollutants. Again due its large bandgap energy, the photocatalytic activity of the material is limited to the ultraviolet region of light [4]. This means that under visible light, the material cannot perform appreciably as a photocatalyst. Its absorption spectrum can be improved or extended into the visible light region by reducing the band gap through doping [22].

2.6 Dyes.

Generally, dyes are either organic or synthetic materials that can adhere inherently to a substrate without the use of additives or by the use of additives. Due to their high affinity to cling to a substrate [60]. They can adhere physically or chemically to the material on which they have been applied. Dye colours are mainly underlined by their chemical structure and are transferred onto substrates by selective absorption of light [60], [61]. Dyes can be classified as natural and synthetic depending on the source. Natural dyes are derived from plants and animals and synthetic dyes are petroleum based compounds [60]. Dyes are used as colourants in leather, fabrics, cosmetics, food items and artistry.

2.6.1 Rhodamine B

Rhodamine B is an organic dye with the molecular formula $C_{28}H_{31}ClN_2O_3$ and a molecular weight of 479.02 g/mol. It also belongs to a family of dyes known as the oxygen-containing heterocyclic xanthene dyes [62]. It serves as a tracer dye especially in water to determine its flow rate and direction of flow. It also serves as a useful ingredient in using some technologies such as fluorescence microscopy and spectroscopy in biomedical sciences [63], [64]. Rhodamine B undergoes degradation either under visible light or ultraviolet light in the presence of a photocatalyst. Without a photocatalyst, degradation of this dye will not occur either under visible or UV light. This indicates the photostability of the dye. In the presence of a photocatalyst, illumination by a light source first causes sensitization of the dye followed by photocatalysis to degrade the dye. The molecular structure of Rhodamine B is shown in Figure 2.4 (Next page).

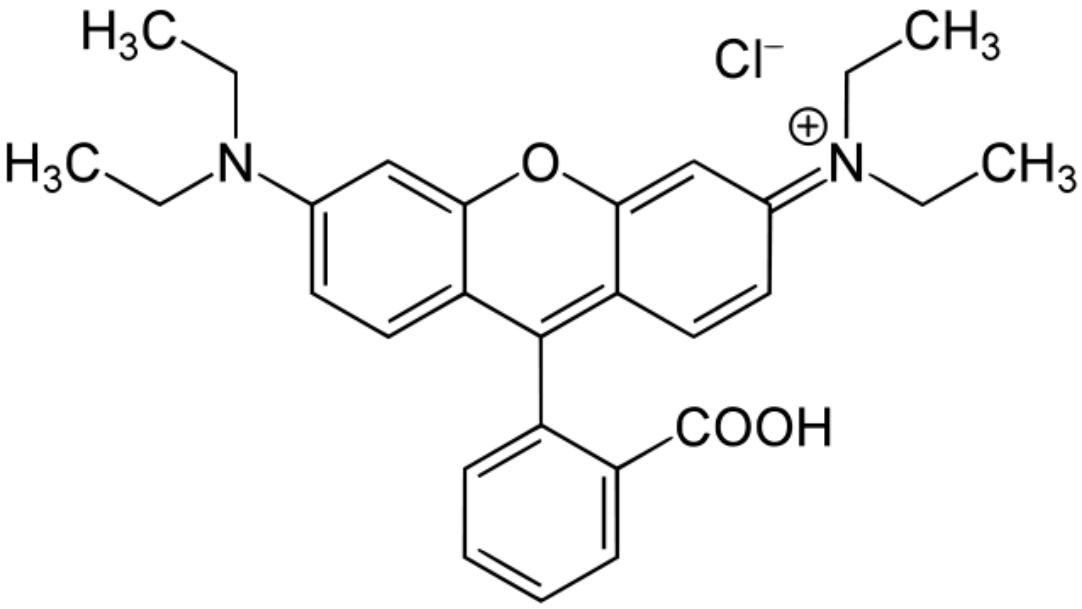

Figure 2.4: Molecular Structure of Rhodamine B.[65]

2.6.2 Methylene Blue.

Methylene Blue is an organic dye with a greenish blue colour that is found in a family of dyes known as phenothiazine. Its molecular formula and molecular weight are $C_{16}H_{18}ClN_3S$ and 319.851 g/mol respectively. It was first discovered in 1876 [31], [66]. It is used to stain certain body tissues and fluids for x-ray diagnosis. In spite of this, it is also used in the leather, paper and textile industries for their products [4], [66].

Methylene blue also behaves as a photosensitizer due to its ability to absorb and transfer light energy to another compound. Its wavelength of absorption of light ranges from $600 - 700$ nm [67].

Methylene blue does not undergo degradation by hydrolysis as well as photodegradation without a photocatalyst. This shows that the dye is photostable and would only degrade by photocatalysis. The molecular structure of Methylene Blue (Figure 2.5) is shown below (next page).

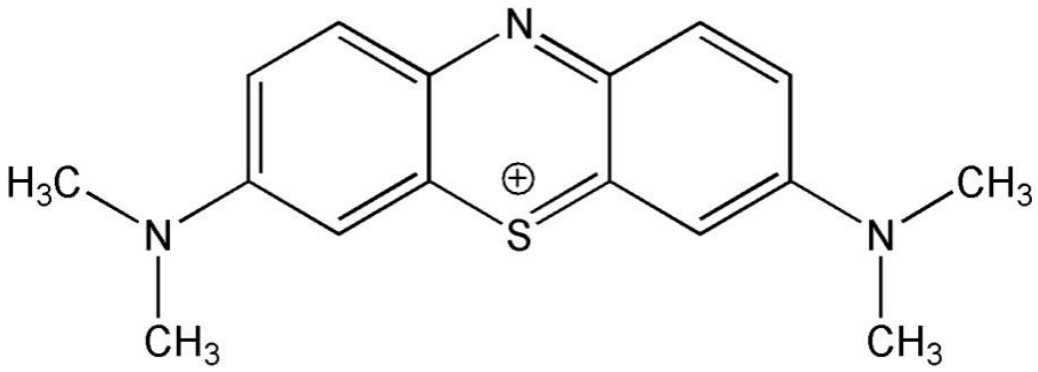

Figure 2.5: Molecular Structure of Methylene Blue [66].

2.7 Other Semiconductor Photocatalysts.

There are other semiconductor materials which can be used for photocatalytic applications. These include titanium dioxide, TiO_2 and zirconium dioxide, ZrO_2.

2.7.1 Titanium Dioxide.

Titanium dioxide is one of the heterogeneous semiconductor materials and the most extensively explored semiconductor photocatalyst over the years [68]. Naturally, it can be extracted from different ores such as ilmenite and leucoxene ores [69]. It exhibits n – type conductivity and has three crystal structures namely rutile, anatase and brookite. The rutile and the anatase has tetragonal crystal system whiles the brookite has the orthorhombic crystal system. At high temperatures the rutile crystal structure exhibits the highest stability followed by anatase and brookite respectively. Consequently, the anatase phase may be obtained at relatively low temperatures compared to the rutile [69], [70]. Generally, TiO_2 has a wide band gap energy which is estimated at 3.0 eV for the rutile phase and 3.2 eV for the anatase phase [69]. This shows that TiO_2 can absorb more light in the UV region than the visible region. However its band gap is tunable by doping with either metallic or non – metallic elements [70][71]. TiO_2 has a number of properties such as biocompatibility, chemical inertness, thermal stability and non – toxicity [72]

which makes it suitable for many applications including bio – sensing, photocatalysis, biomaterials and photonics. For photocatalytic applications the anatase phase of TiO_2 is usually suitable since it has the tendency to generate electron – hole pairs and can also be easily synthesized. Synthesis techniques for TiO_2 nanoparticles include sol – gel, hydrothermal, solvothermal and ultrasonic synthesis [69].

2.7.2 Zirconium Dioxide.

Zirconium dioxide is also a semiconductor material which has also received considerable attention relating to photocatalytic applications. Its photocatalytic activity has been explored in a number of studies including the photocatalytic gas-phase oxidations of methanol and hexane [73]. ZrO_2 has a wide band gap which ranges between 3.25 eV and 5.1 eV [74]. ZrO_2 exhibits good properties such as thermal stability, chemical inertness, high specific surface area and good optical properties such as photoactivity that make it suitable for photocatalytic applications [73]. For effective photocatalytic activity, ZrO_2 must be porous and more crystalline development in order to enhance its light harvesting tendencies, reduce occurrence of recombination, and increase the number of surface active sites [73]. Zirconium dioxide shows three different polymorphs namely; monoclinic, tetragonal and cubic [74]. Naturally, it exists in the monoclinic phase and assumes the tetragonal and cubic phases at higher temperatures. It can be synthesized using techniques such as hydrothermal, sol – gel, and thermal decomposition [74].

CHAPTER THREE

3.0 Experimental Design.

3.1 Chemicals.

The reagents used in this work were Zinc acetate, Oxalic Acid, Ethanol (99 %), Rhodamine B and Methylene Blue and were obtained from Loba Chemie Ltd (India) All the reagents used in this work were of analytical grade and were used as received without additional purification.

3.2 Synthesis of ZnO Nanoparticles via Sol-Gel.

ZnO nanoparticles were synthesized using the Sol-gel method. In a typical experiment, 0.01 mol of zinc acetate dehydrate was dissolved in 60 ml of absolute ethanol and stirred at 65°C for 30 minutes to obtain a clear solution. Oxalic acid solution was also prepared by dissolving 0.04 mol of oxalic acid dehydrate in 80 ml of ethanol and stirred for 30 minutes at 55 °C. The Oxalic acid solution was then added to the zinc acetate solution dropwise at 65°C and stirred continuously for 1 hour. A white sol is obtained which was aged to form a gel, dried at 80 ℃ in an oven for 24 hours. The aerogel obtained was calcined at different temperatures: 400 ℃, 500 ℃ and 600 ℃ for 5 hours to obtain ZnO nanoparticles. The prepared ZnO nanoparticles were then subjected to various characterization techniques and was also used for photocatalytic experiments.

Below is flow chart (Figure 3.1) depicting the summary of the process that was undertaken to synthesize ZnO nanoparticles. Images of the processes taken at the laboratory are also shown in Figure 3.2 below (pages 21).

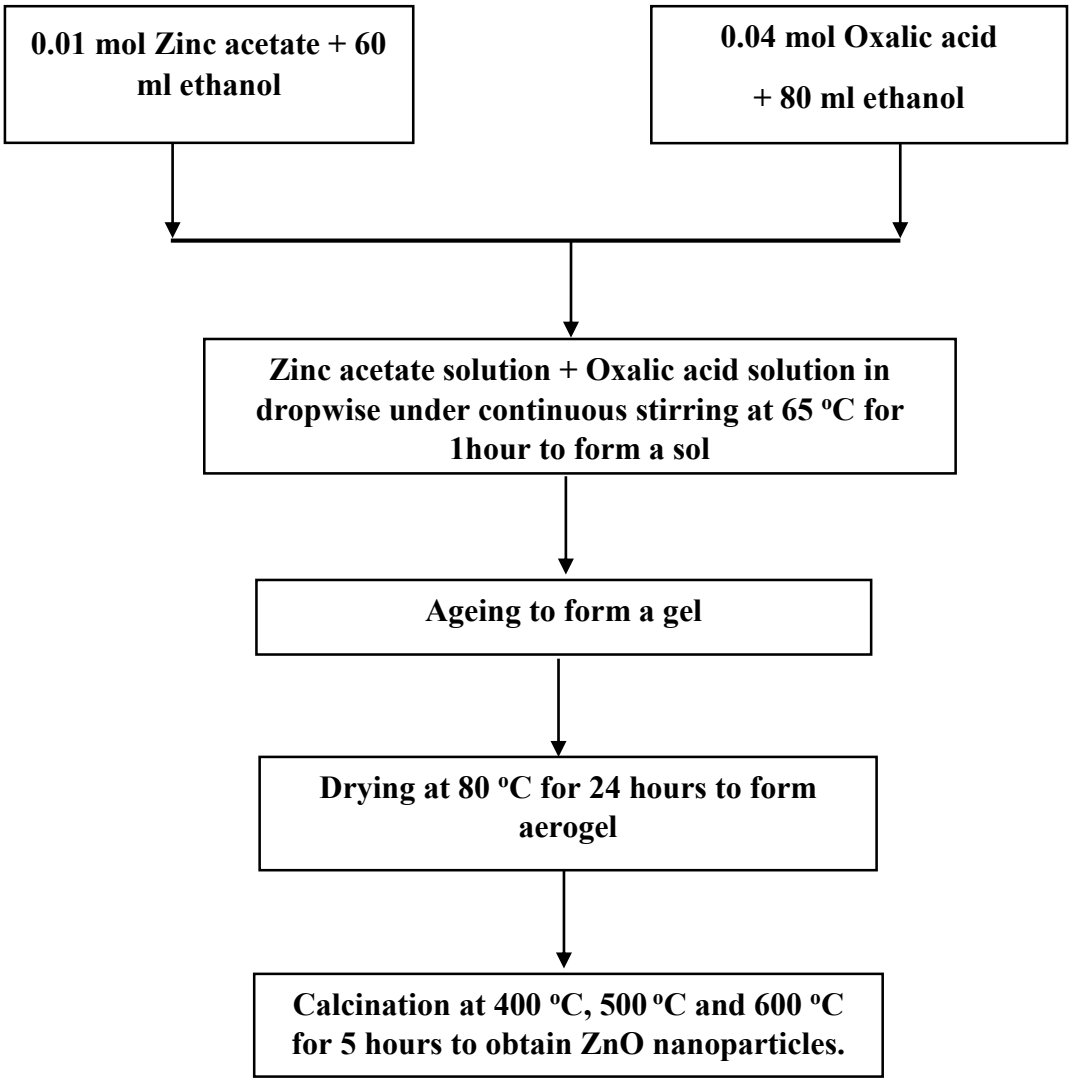

Figure 3.1: Preparation of zinc oxide nanoparticles via Sol-gel method.

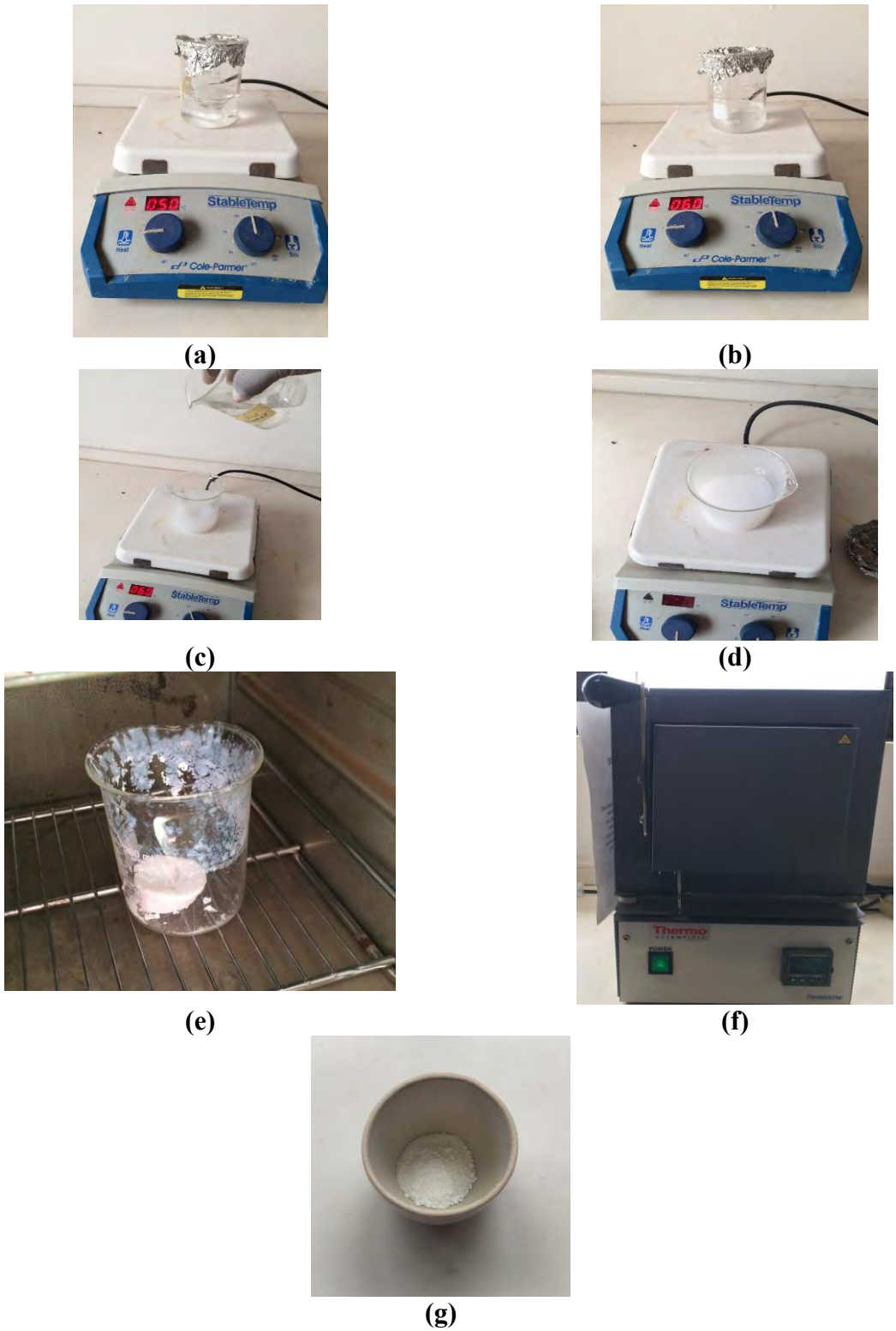

Figure 3.2. ZnO synthesis: Stirring of oxalic acid solution (a) Stirring of zinc acetate solution (b) Addition of oxalic acid in dropwise to zinc acetate solution under magnetic stirring (c) Ageing

process (d), Drying of xerogel in oven (e) Calcination process using furnace (f) ZnO particles after calcination (g)

3.3 Characterization of Zinc Oxide Nanoparticles.

Characterization techniques used to analyze Zinc oxide nanoparticles include X-Ray Diffraction (XRD), Scanning Electron Microscopy (SEM), Fourier Transform Infra-Red (FTIR), and UV-vis Spectrometry.

3.3.1 X-Ray Diffraction

To determine the crystal structure and the crystallite size of the prepared ZnO nanoparticles, X-ray diffraction analysis was carried out using an X-ray diffractometer (Empyrean Diffractometer Panalytical BV, Netherlands) as shown in (**Figure 3.3**). The particles were bombarded x-ray radiations from Cu Kα of wavelength (1.5406 Å) in a 2θ scan range of 20º–80°. The ZnO nanoparticles crystallite size was estimated using the Scherer equation:

$$D = \frac{K\lambda}{\beta\cos\theta} \quad \ldots\ldots\ldots\ldots\ldots\ldots\ldots\ldots\ldots\ldots\ldots\ldots \quad 3.1$$

Where K is the Scherer constant (K=0.89), λ is the X-ray wavelength, β is the peak width of the half maximum and θ is the Bragg diffraction angle.

Figure 3.3: X-Ray Diffractometer

3.3.2 Scanning Electron Microscopy.

The surface morphology of zinc oxide nanoparticles were analyzed using the Scanning Electron Microscope (FEI Nova NanoSEM). Zinc oxide nanoparticles were bombarded with a primary electron beam accelerated and the secondary electrons obtained were used to visualize the microstructure of the samples which gave images captured on a computer.

3.3.3 FTIR Spectroscopy.

Fourier Transform Infrared Analysis was done on the prepared zinc oxide nanoparticles in the range of 4500 to 400 cm^{-1} to ascertain the presence of zinc in the material and oxygen molecules adsorbed onto the surface of zinc in the preparation process using the PerkinElmer Spectrum Two FTIR machine. FTIR was also used to investigate the potential existence of other functional groups in the prepared material.

3.3.4 UV-Vis Spectrometry.

To determine the absorption spectrum of ZnO nanoparticles, the nanoparticles were subjected to UV-vis spectrometry using a spectrophotometer (GENESYS 10S UV-Spectrophotometer). This was done by dispersing 5 mg of ZnO nanoparticles in 50 ml distilled water and transferring the mixture into a cuvette for the photo analysis. The cuvette was then placed in the spectrophotometer and scanned to record the absorbance of light by the material. The analysis was carried over a wavelength range of 200 nm to 900 nm. The Tauc plot was used to estimate the band gap energy of zinc oxide nanoparticles. This was done by plotting a graph of $(\alpha hv)^2$ against hv where $= \frac{2.303\ A}{d}$, A is the absorbance, d is the thickness of the material, h is Planck's Constant and v is the frequency of light absorbed.

3.4 Photocatalytic Experiment.

Photocatalytic experiment carried out for the degradation of Rhodamine B and Methylene Blue was done using ultraviolet light with ZnO nanoparticles as the photocatalyst.

3.4.1 Photocatalytic Degradation Experiment for Rhodamine B.

I. Rhodamine B dye solution was prepared by dissolving 0.01 g of dye in 1litre distilled water and stirred continuously to attain form a homogeneous mixture.
II. 0.1 g of the catalyst (ZnO nanoparticles) was added to 100 ml of the dye solution in a 250 ml beaker to form a dye-catalyst mixture.
III. The dye-catalyst mixture was stirred rigorously in the dark for 1hour to obtain adsorption-desorption equilibrium.

IV. The mixture was then exposed to a bench top Ultraviolet light irradiation source (UV transluminator, 330 W)

V. The mixture was swirled at every 5 minutes interval whiles it was exposed to the UV light.

VI. About 3 ml of the mixture was taken at every 20 minutes interval for a period of 160 minutes with a syringe, centrifuged to separate nanoparticles from the dye solution and analyzed in a UV-vis Spectrometer and the absorbance at wavelength 555 nm was recorded.

3.4.2. Photocatalytic Degradation Experiment for Methylene Blue.

I. Methylene Blue dye solution was prepared by dissolving 0.01 g of dye in 1litre distilled water and stirred continuously to attain form a homogeneous mixture.

II. 0.1 g of the catalyst (ZnO nanoparticles) was added to 100 ml of the dye solution in a 250 ml beaker to form a dye-catalyst mixture.

III. The dye-catalyst mixture was stirred rigorously in the dark for 1hour to obtain adsorption-desorption equilibrium.

IV. The mixture was then exposed to a bench top Ultraviolet light irradiation source (UV transluminator, 330 W)

V. The mixture was swirled at 5 minutes interval whiles it was exposed to the UV light.

VI. About 3 ml of the mixture was taken at every 20 minutes interval for a period of 160 minutes using a syringe. The mixture taken was centrifuged at 5000 rpm for 5 minutes to separate the particles from the dye and the supernatant was analyzed in a UV-vis Spectrometer at a wavelength of 665 nm.

The photocatalytic degradation process is shown in a flow chart (**Figure 3.4**) below. Images of the laboratory process undertaken for the photocatalytic degradation experiment are also shown in **Figure 3.5** (next page).

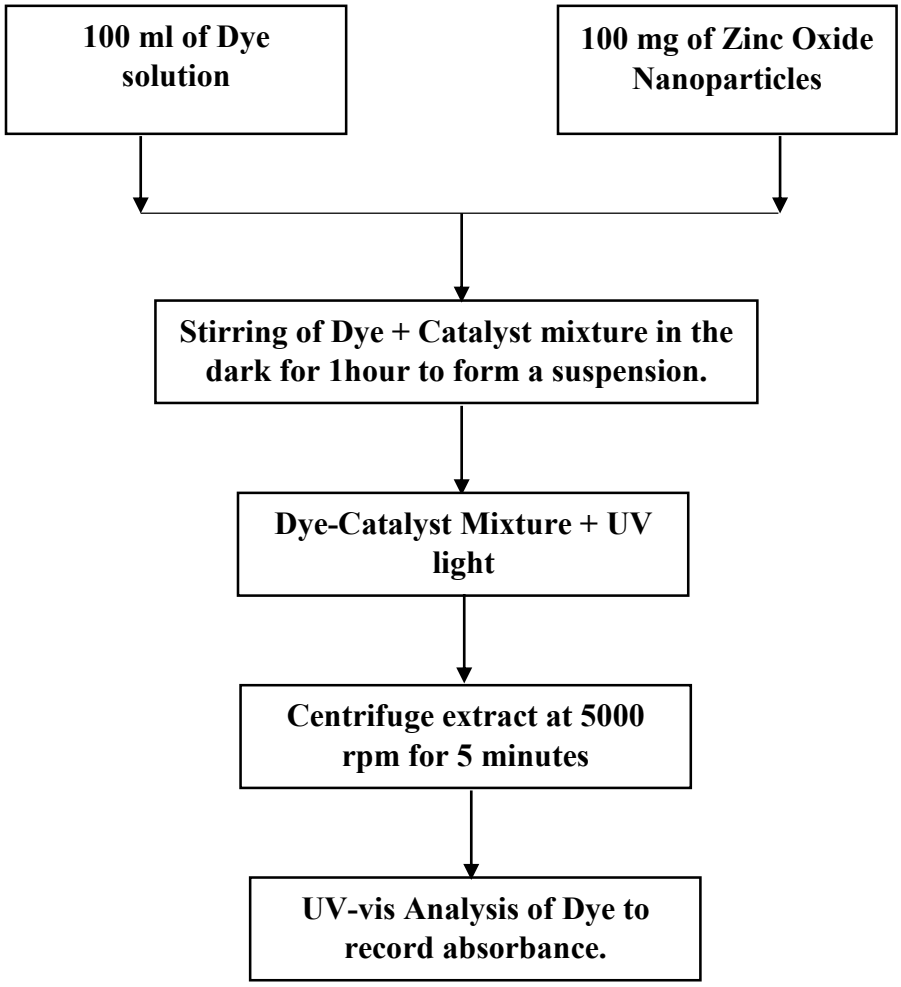

Figure 3.4: Photocatalytic Degradation Process

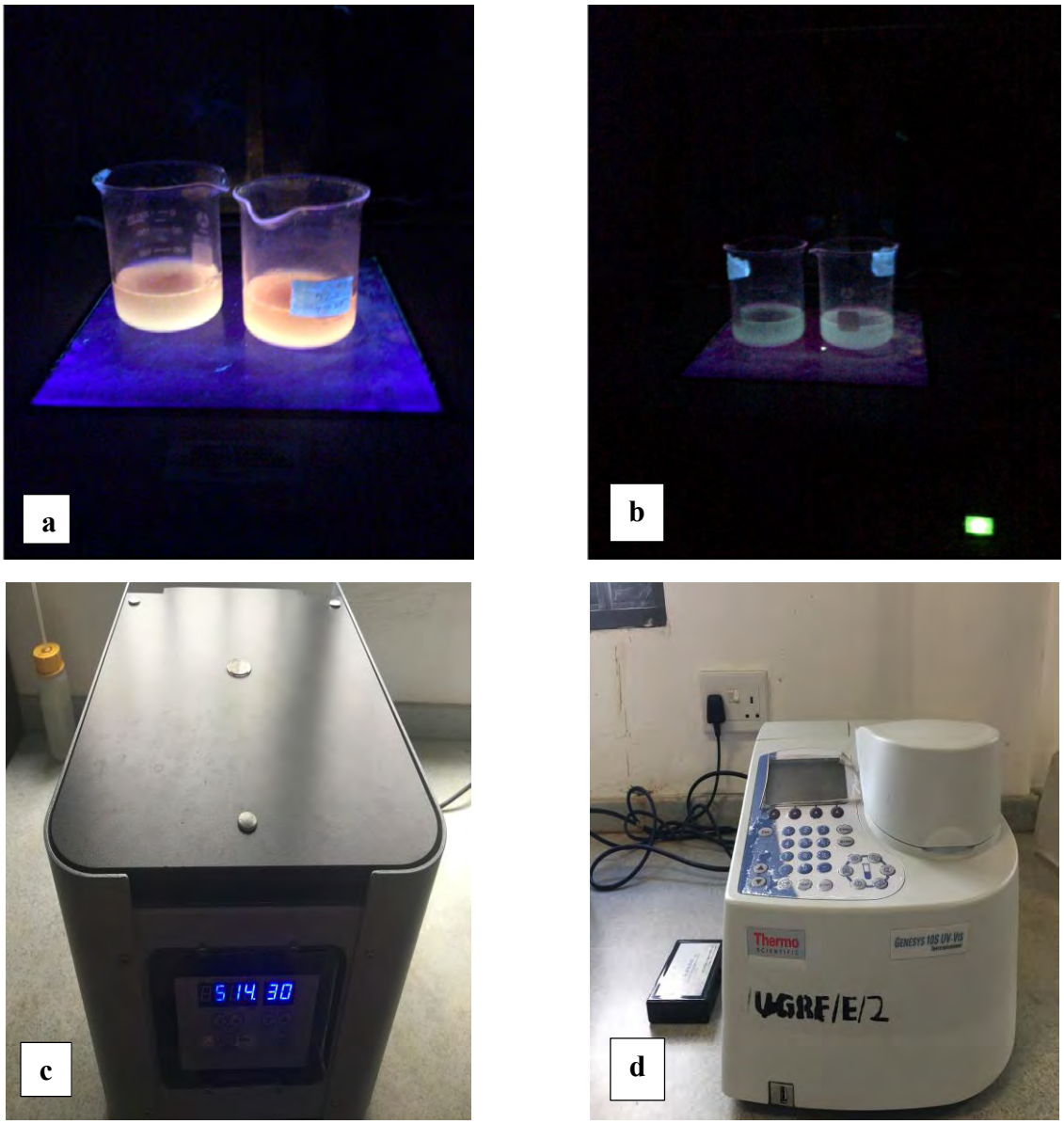

Figure 3.5: Process of photocatalysis: (a) Mixture of RhB and ZnO under UV irradiation (b) Mixture of MB and ZnO under UV irradiation (c) Centrifuge (d) UV-Vis Spectrophotometer.

3.4.3 Effects of Catalyst Load Experiment.

The catalyst load effect on the rate of degradation of Methylene blue and Rhodamine B was investigated by performing photocatalytic experiment on both dyes using different amount of catalyst in each experiment. The amount of catalyst was increased from 0.1 g to 0.3 g with an

increment of 0.05 g for each experiment. Five different experiments were done. The volume of the dye solution was held at 100 ml for all experiments. The photocatalytic degradation process as shown in **Figure 3.4** was followed for each experiment.

3.4.4 Photostability Experiment of ZnO Nanoparticles.

The photostability of ZnO nanoparticles in photocatalytic degradation of Methylene Blue and Rhodamine B was also investigated by performing four cycles of photodegradation using 0.2 g of ZnO nanoparticles as catalyst. The catalyst (ZnO nanoparticles), after each cycle was centrifuged, washed with distilled water and dried in air to be used for the next cycle. This was done to maintain the same nanoparticles throughout the four cycles of photocatalytic experiment and also to ascertain the potential of the catalyst to be recycled or reused for several photocatalytic reactions.

CHAPTER FOUR

4.0 Results and Discussions

4.1 ZnO nanoparticle Synthesis.

In the synthesis of ZnO nanoparticles via sol-gel method, a solution of oxalic acid and 80 ml ethanol (99 %) was added in dropwise to a solution of zinc acetate and 60 ml ethanol in a molar ratio of 4:1 for Oxalic acid and zinc acetate respectively. A white sol was formed upon mixing the solutions. The sol was aged, dried at 80 ℃ in an oven and calcined to obtain white crystalline ZnO nanoparticles. The equation below illustrates the reaction that took place in the sol-gel process.

$Zn\ (CH_3COO)_2.\ 2H_2O + H_2C_2O_4.2H_2O \rightarrow ZnC_2O_4.2H_2O + 2CH_3COOH$…….. (4.1)

$ZnC_2O_4.2H_2O \rightarrow ZnO + CO + CO_2 + 2H_2O$…… (4.2)

4.2 XRD Analysis

The XRD patterns for the various samples synthesized at different calcination temperatures were obtained using (Empyrean Diffractometer Panalytical BV) to characterize the crystal phases and degree of crystallinity of ZnO nanoparticles. All the peaks detected and indexed are characteristic of the ZnO wurtzite structure as shown in Figure 4.1 with characteristic 2θ values at 31.81°, 34.44°, 36.31°, 47.602°, 56.62°, 63.01°, 66.48°, 67.97°, and 69.19° corresponding to the (100), (002), (101),(102), (110), (103), (200), (112), and (201) planes, respectively[68]. The estimated crystallite sizes of all samples were calculated using the Scherer equation: $D = \frac{K\lambda}{\beta\cos\theta}$ where k, Scherer constant (0.89), X-ray wavelength (0.154 nm), Bragg diffraction angle θ corresponding to ZnO (101) reflection at 36.30°, respectively and the FWHM for all samples were estimated

using origin software. The FWHM of samples at different calcination temperatures and their corresponding crystallite size are shown in Table 4.1 below.

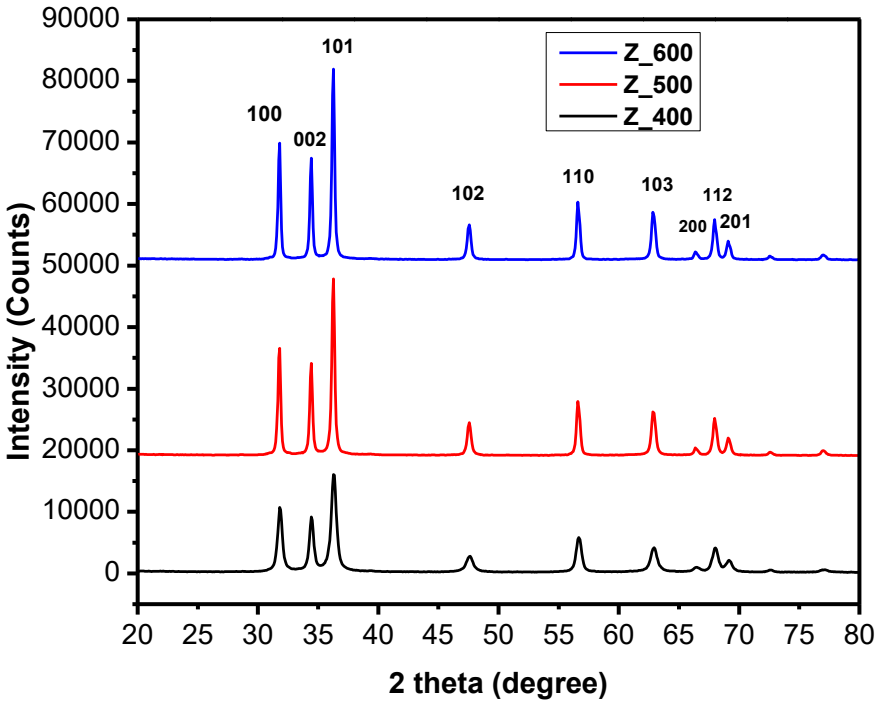

Figure 4.1: X-ray diffraction patterns of ZnO nanoparticles calcined at 400°C, 500°C and 600°C

Table 4.1: Crystallite size of ZnO nanoparticles at different calcination temperatures and their respective FWHM.

Calcination Temperature °C	Full Width at Half Maximum (FWHM)	Crystallite Size (nm)
400	0.544	16
500	0.314	28
600	0.290	30

The crystallite size of ZnO nanoparticles calcined at a temperature of 400 °C was 16 nm, representing the smallest among all the three samples whereas 28 nm and 30 nm were the estimated crystallite sizes at calcination temperatures of 500°C and 600°C respectively. It is observed that crystallite size increased with increased calcination temperatures. This is an indication that particle

size growth rate increases at higher temperatures resulting in the formation of large grain sizes. Also the crystallinity of ZnO particles increase as the calcination temperature increases and this can be seen in the sharpness of peaks at higher temperatures.

Modelled XRD results obtained for ZnO samples calcined at 400 °C, 500 °C, and 600 °C using Whole Powder Pattern Modelling (WPPM) method on a PM2K software showed good fitting between the experimental peaks and the calculated peaks as shown in Figure 4.2. The baseline of all the three graphs is almost flat, indicating that there is no or little significant difference between the experimental and the calculated peaks of the zinc oxide nanoparticles.

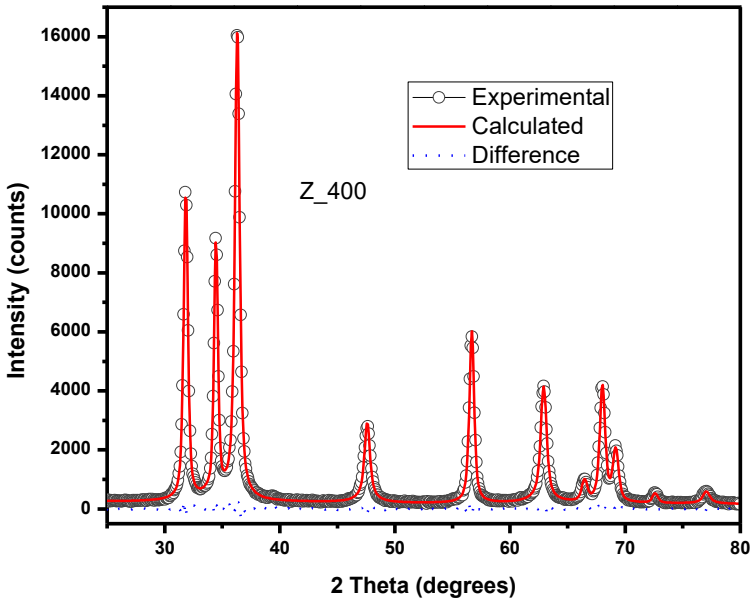

(a)

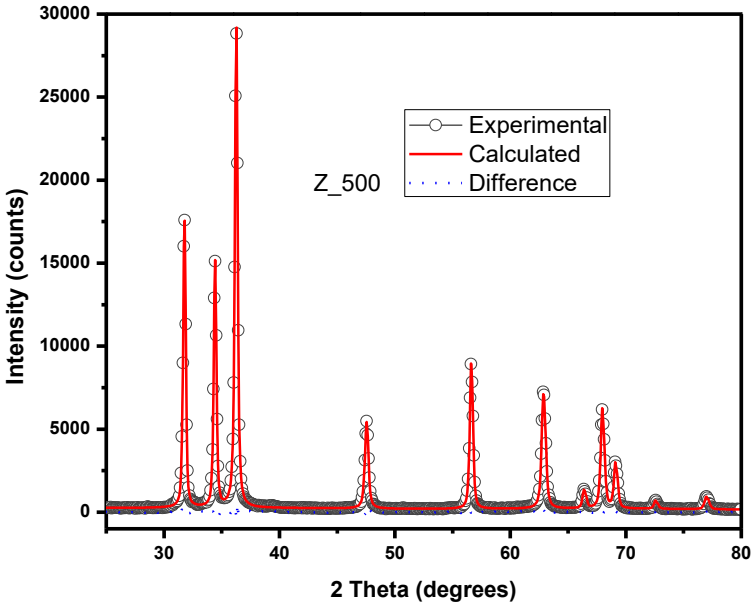

(b)

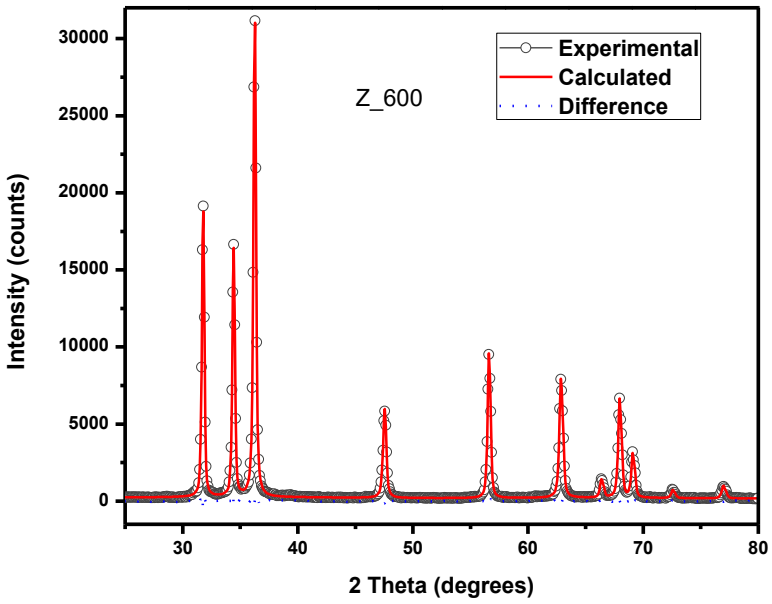

(c)

Figure 4.2: Modelled XRD patterns of ZnO nanoparticles calcined at (a) 400 °C (b) 500 °C, (c) 600

4.2.1 Grain Size Analysis.

The Grain size of the synthesized zinc oxide nanoparticles were analyzed from the XRD results using Whole Powder Pattern Modelling Method (WPPM) supported on PM2K Software. The model was used to estimate the average grain size of ZnO nanoparticles synthesized at different calcination temperatures. A graph of average grain size against temperature was obtained. The average grain size increased as the temperature also increased as shown in **Figure 4.3**. This can be attributed to increased grain growth in a material when subjected to high temperature treatment.

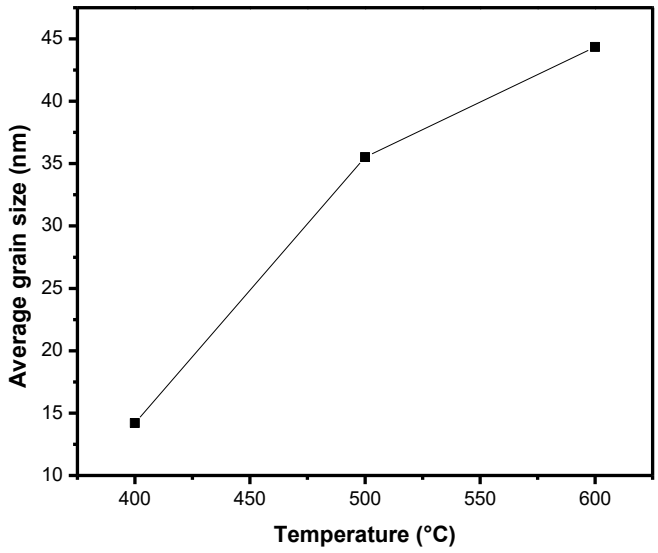

Figure 4.3: Average grain size against temperature for ZnO nanoparticles.

4.2.2 Grain Size Distribution.

The grain size distribution in the synthesized ZnO nanoparticles as obtained by WPPM method using PM2K Software was done to investigate the predominant grain sizes in the material. A lognormal size distribution was obtained from the modelled XRD patterns. (**Figure 4.4** Next page)

The predominant grain size of zinc oxide nanoparticles calcined at 400 ℃ is 14.2 nm, 32 nm for 500 ℃ and 42 nm for 600 ℃ and this is in respect to the maximum frequency observed on the graph. A broad curve is observed for Zinc oxide nanoparticles calcined at 400 ℃ and 500 ℃ and this shows that more grains were grown in the material as the temperature was increased.

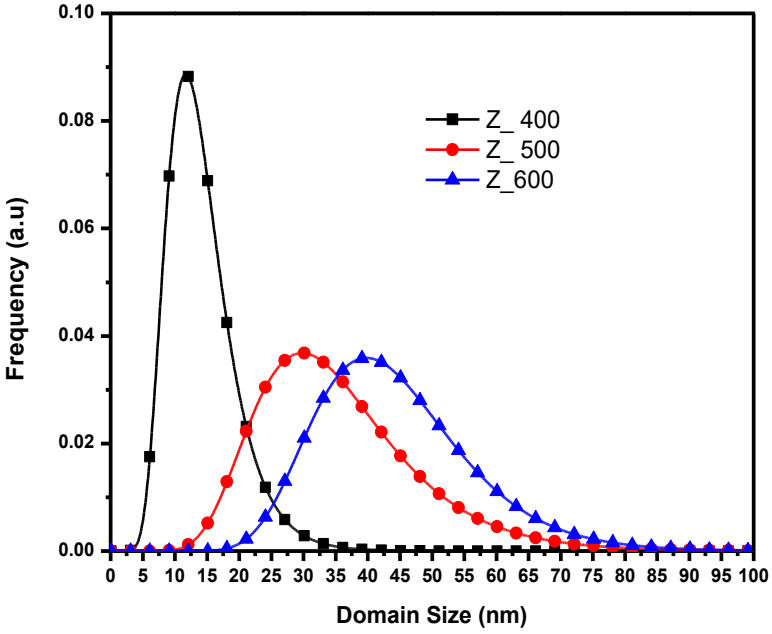

Figure 4.4: A lognormal size distribution of synthesized ZnO nanoparticles.

4.3 FTIR Analysis.

FTIR spectra of ZnO nanoparticles calcined at different temperatures (400 ℃, 500 ℃ and 600 ℃) are shown in Figure 4.2. This characterization was done to determine the presence of zinc and oxygen molecules in the prepared zinc oxide nanoparticle and other functional groups that might be present. Fingerprint bands observed at 861 cm^{-1} and 688 cm^{-1} represent the inter-atomic

vibrations of $Zn - O$ bond. These bands are also characteristic of the metal zinc since bands of metals are usually observed below 1000 cm^{-1} [75]. The bands observed at 3400 to 3500 cm^{-1} are due to $O - H$ (hydroxyl group) bond stretching and deformation owing to the molecules of water adsorbed onto the surface of zinc. A decrease in the intensity of the band is observed as the calcination temperature was increased from 400 ℃ to 600 ℃. This is an indication that more water molecules leave the sample at higher temperatures. Bands stretching from 2400 cm^{-1} to 1300 cm^{-1} represent $O = C = O$ and $C = O$ bonds as a result of carbon dioxide adsorption from the atmosphere during synthesis [76], [77].

It is also observed that there is a negligible shift to a lower wavenumber due to increase in the calcination temperature. This shift can be related to a change in the lattice parameters of the ZnO nanoparticles [78].

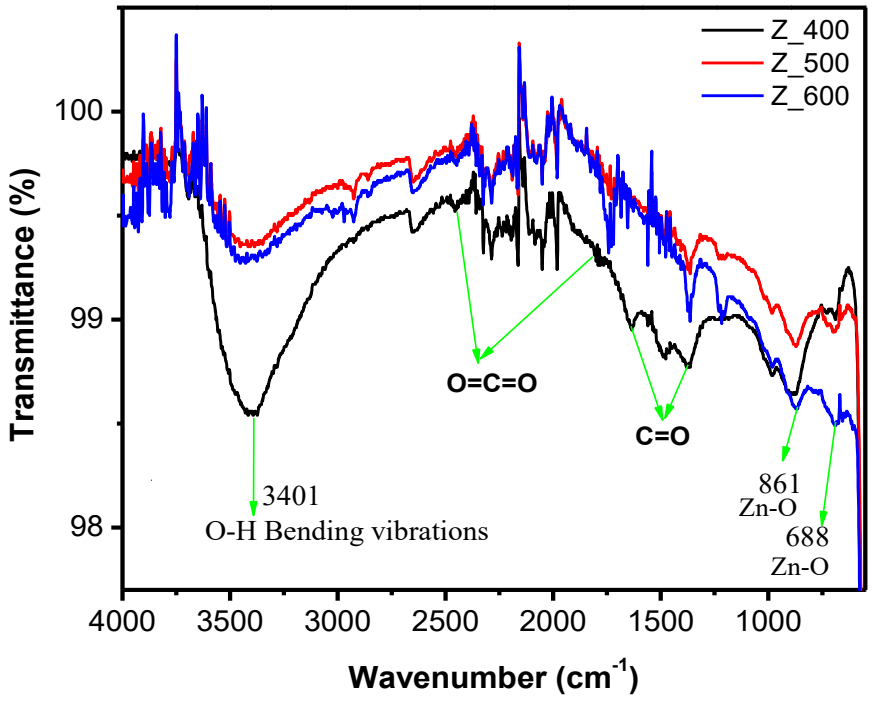

Figure 4.5: FTIR Spectra of ZnO nanoparticles

4.4. UV-Vis Spectra.

The UV–vis absorption spectra of the ZnO nanoparticles calcined at different temperatures of 400 ℃, 500 ℃ and 600 ℃ are shown in **Figure 4.5** (Next page). It is observed that the main absorption peak for all the three samples is below 400 nm. This peak is characteristic of the wavelength at which zinc oxide absorbs photons of light and this is due to the band gap energy of the material. This peak is observed at 370 nm for Z_400 and 375 nm for both Z_500 and Z_600 indicating a slight increase in the absorption peak as the calcination temperature is increased. This can be attributed to the intrinsic band gap absorption of ZnO due to the electron transitions from the valence band to the conduction band.

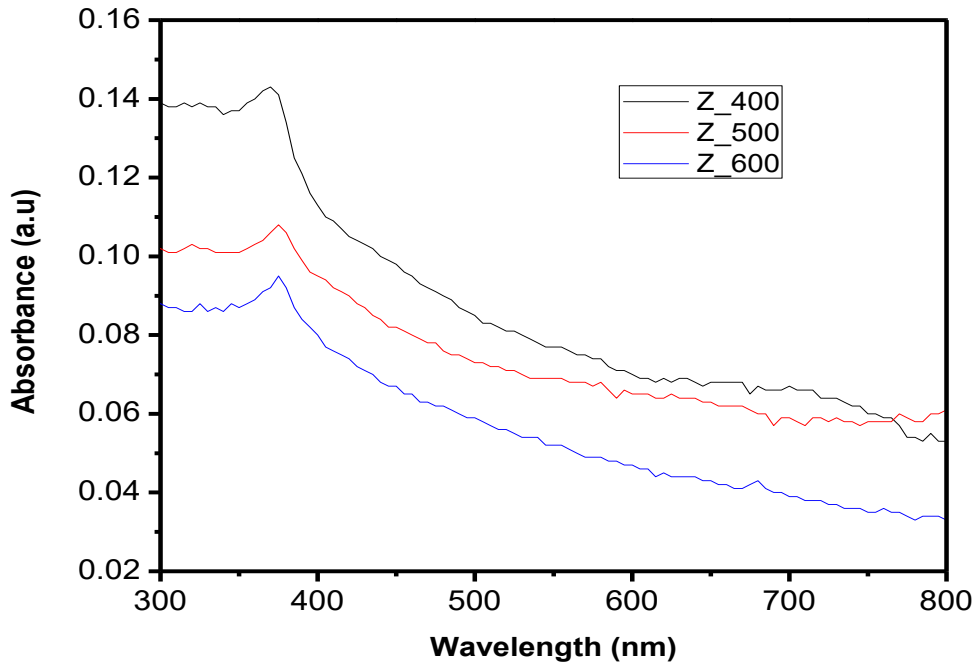

Figure 4.6: UV-vis spectra of ZnO nanoparticles.

4.4.1 Band Gap Estimation.

From the UV-vis spectra, the bandgap energy of the synthesized ZnO nanoparticles were estimated using the Tauc Plot. A graph of $(\alpha hv)^2$ $against$ hv was plotted, where α is the absorption coefficient of the material. The absorption coefficient is the amount of radiations absorbed by the material with respect to its thickness. The absorption coefficient $\alpha = \frac{2.303\,A}{d}$, where A is the absorbance and d is the thickness of the material. A tangent to the curve is extrapolated to the x-axis to read the band gap energy of ZnO nanoparticles as shown in **Figure 4.7**. The tangent was taken at the point where the curve begins to linearize.

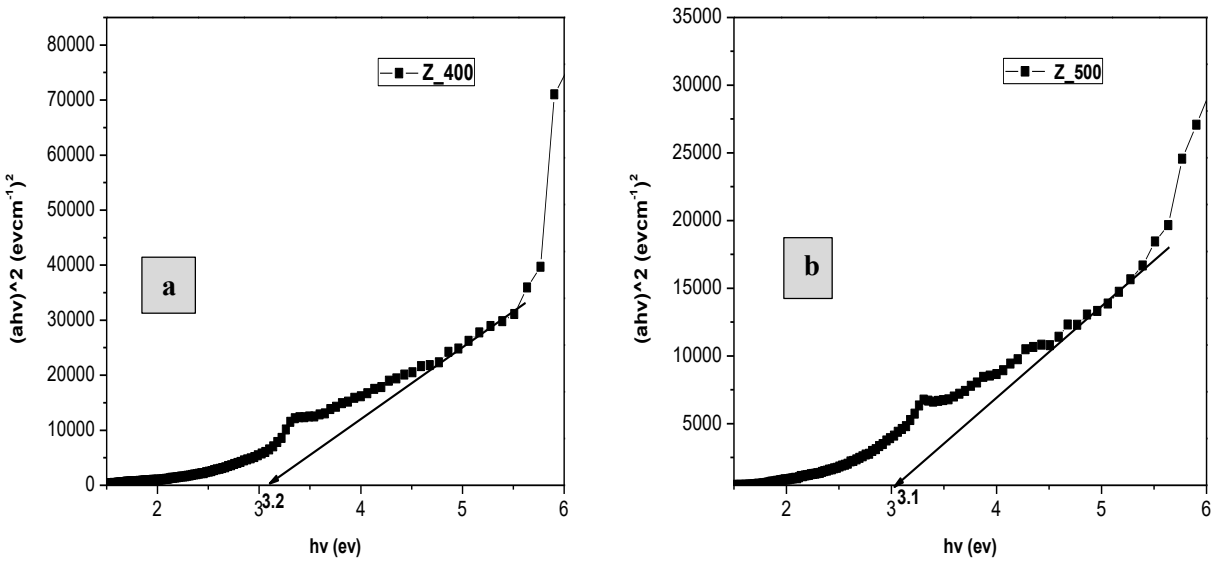

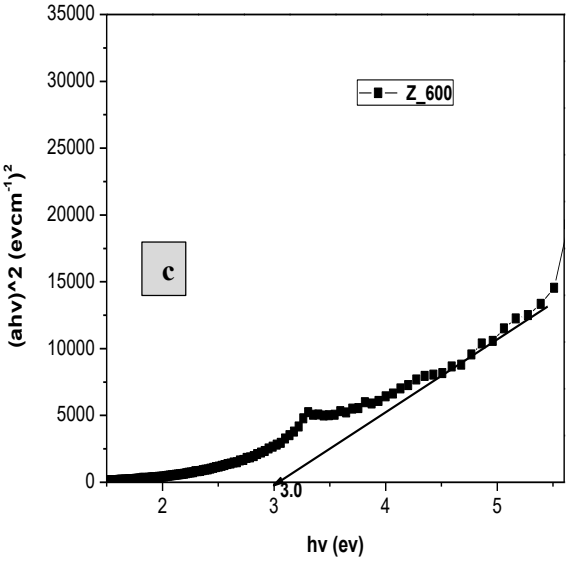

Figure 4.7: Tauc plot of Zinc oxide nanoparticles synthesized at (a) 400 ℃ (b) 500 ℃ and (c) 600 ℃

A decrease in bandgap energy was observed for ZnO nanoparticles as the calcination temperature was increased from $400 - 600$ degree Celsius. This is attributed to the increase in the vibrational amplitude of electrons at higher temperatures. It can also be attributed to quantum size effect where smaller crystallite size materials have high confinement of electrons in the energy levels resulting in an increase in the band gap [75]. Therefore, band gap energy for ZnO nanoparticles increases with decreasing crystallite size due to quantum size effect and decreases with increasing temperature due to electrons vibrational amplitude.

4.5 Scanning Electron Microscopy.

The micrograph obtained from the SEM of zinc oxide nanoparticles calcined at different temperatures show rice-like or fibrous microstructure morphology for all three samples. Particle agglomeration is observed for zinc oxide nanoparticles calcined at all temperatures but increased with increasing temperature resulting in a more clustered structure as observed at 600 ℃. This is

due to the high rate of nucleation and grain growth at higher calcination temperatures. The SEM images are shown in Figure 4.8 below.

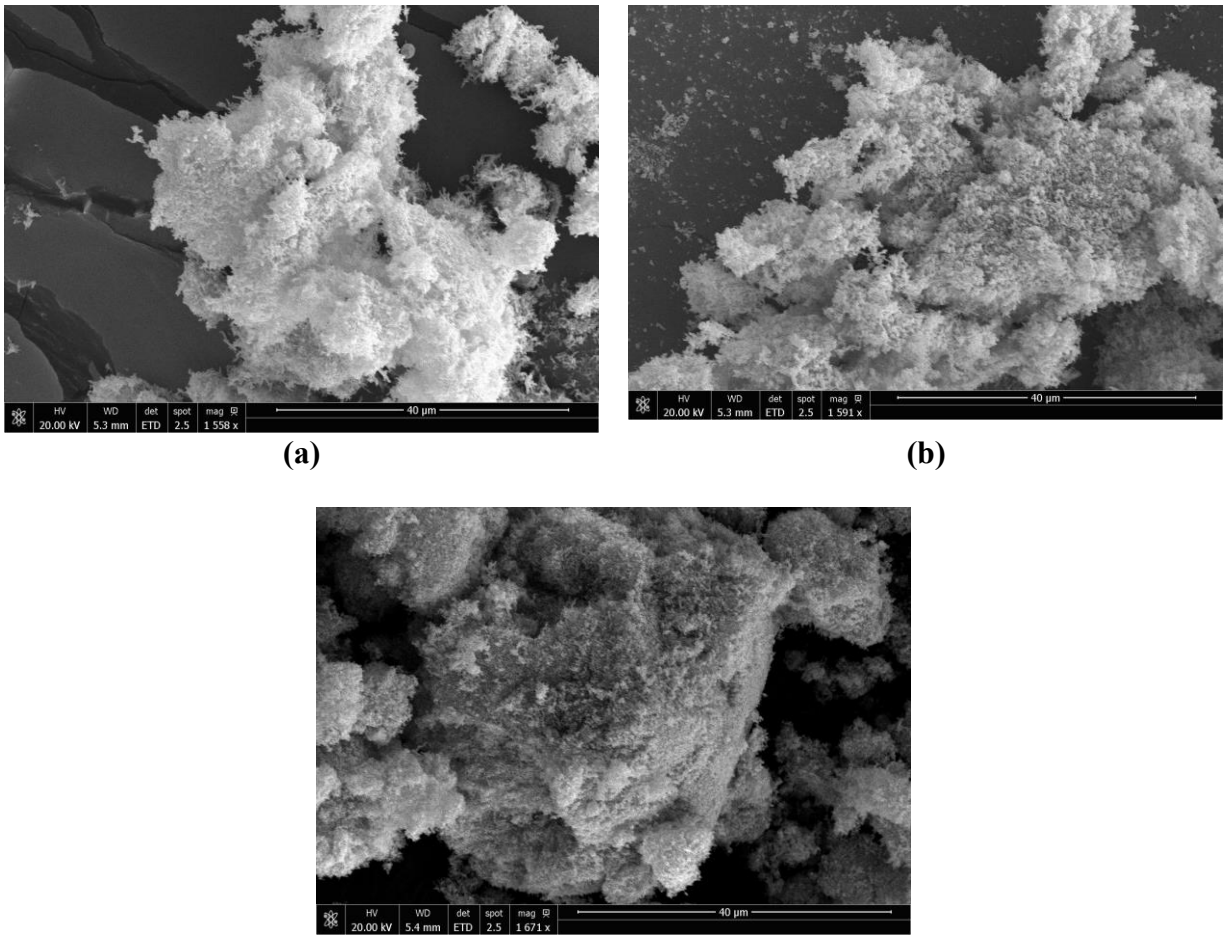

Figure 4.8: SEM images of ZnO nanoparticles calcined at (a) 400 ℃ (b) 500 ℃ (c) 600 ℃

4.6 Photocatalytic Degradation.

Photodegradation of Rhodamine B and Methylene Blue was carried out with the use of zinc oxide nanoparticles in the presence of ultraviolet light sourced from a UV transluminator of 330 W. The

photodegradation of both dyes were successful as reduction in initial concentration was observed for both dyes at the end of 160 minutes. Also decolourization of the dyes were observed at the end of the experiment **(as shown in Figure 4.9)** and this is an indication that the dyes were removed by photocatalytic reaction. This shows that the catalyst (ZnO nanoparticles), in the presence of light generated electron-hole pairs which migrate to its surface to initiate the reaction. Hydroxyl radicals and superoxide radicals are produced when holes combine with hydroxyl groups and electrons combine with oxygen on the surface of the catalyst respectively. The radicals constitute the major species that oxidize Rhodamine B and Methylene Blue into green products such carbon dioxide, water and mineral acids.

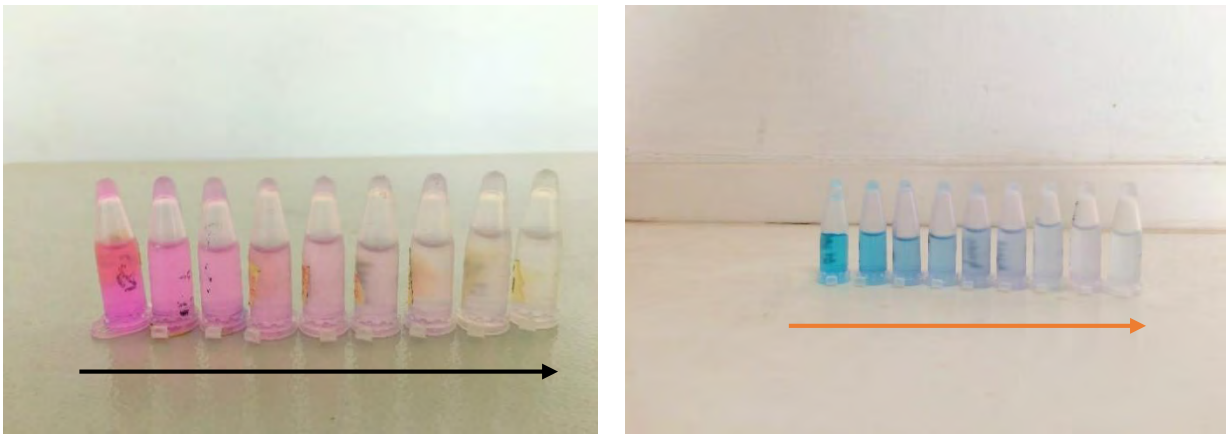

From 0 – 160 minutes
(a)

From 0 – 160 minutes
(b)

Figure 4.9. Decolourization of RhB and MB as a result of photodegradation. (a) RhB (b) MB.

4.6.1 Photodegradation of Rhodamine B.

The photodegradation of Rhodamine B was done using ZnO nanoparticles calcined at different temperatures and a UV light source for 160 minutes. Photodegradation of Rhodamine B was seen

in the decrease in the initial concentration of the dye and the decolourization of the dye after being exposed to UV light in the presence of ZnO nanoparticles for 160 minutes. Two control experiments were conducted to investigate the factors necessary for photodegradation to occur. By this, 100 ml of Rhodamine B dye without catalyst was irradiated with UV light for 160 minutes. At the end of 160 minutes of irradiation, significant degradation was not observed. Also, in the second experiment, 100 ml of the dye containing 100 mg of the catalyst was placed in a dark room for 160 minutes without UV irradiation. It was also observed that no significant degradation took place at the end of the experiment. This is an indication that both catalyst and UV light are necessary for degradation to occur. The photodegradation curve of Rhodamine B using ZnO nanoparticles calcined at different temperatures are shown in Figures (4.10, 4.11 and 4.12). From the graphs, it is observed that, absorbance at the 160th minute is the minimum for all samples. The lowest absorbance value at 160 minutes was achieved using Z_400 followed by Z_500 and Z_600 respectively. This shows that particles calcined at 400 ℃ are the most effective and this is attributed to the size of the particles obtained.

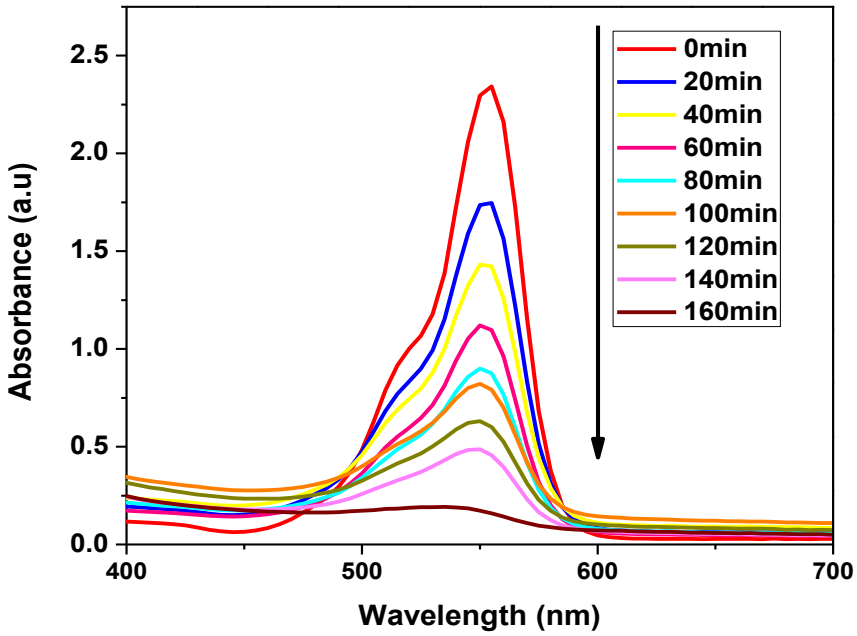

Figure 4.10: Photodegradation of RhB using Z_400

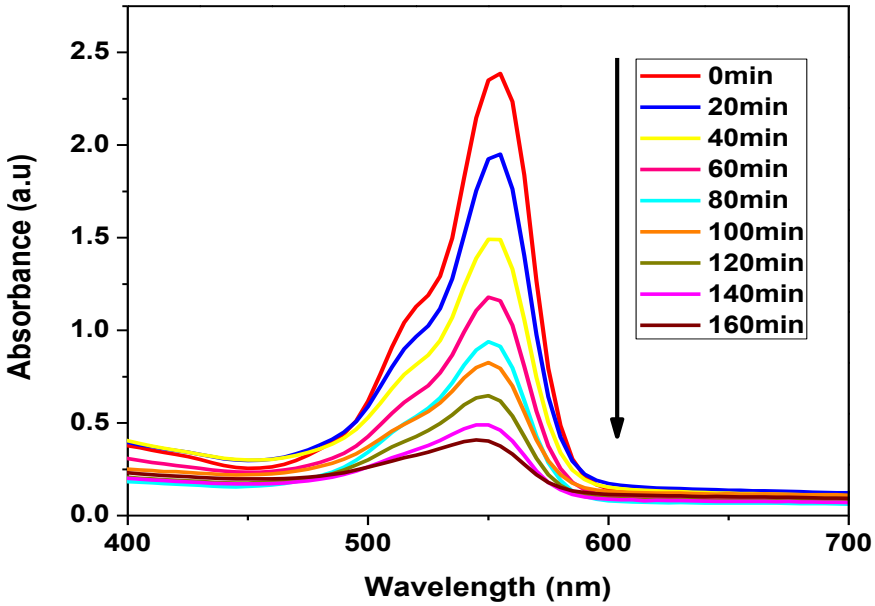

Figure 4.11: Photodegradation of RhB using Z_500

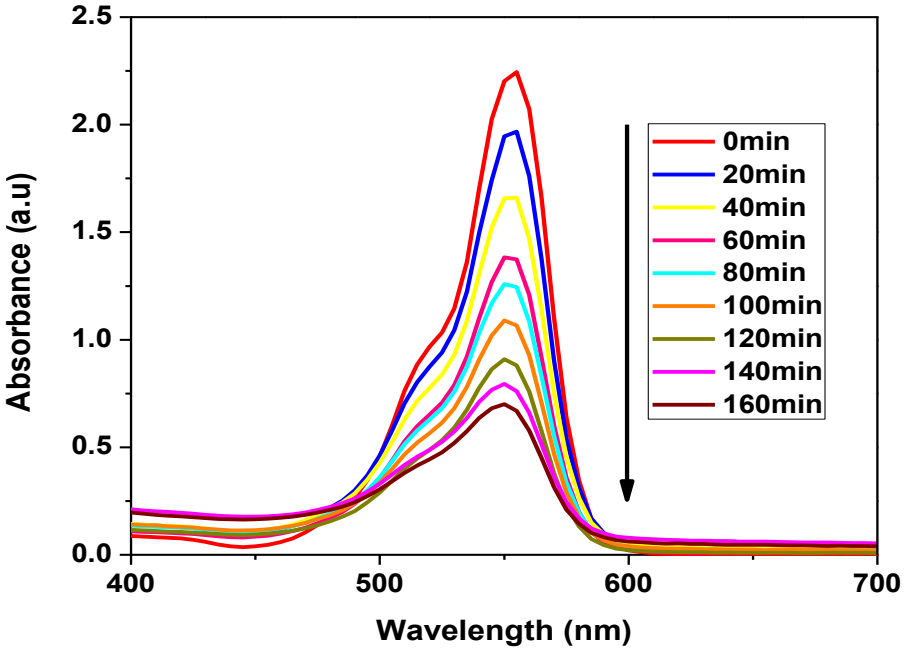

Figure 4.12: Photodegradation of RhB using Z_600

Figures 4.13 and 4.14 below also depicts the degradation of the Rhodamine B dye without catalyst and Rhodamine B dye containing catalyst without UV light irradiation respectively. No significant degradation was observed at the end of 160 minutes.

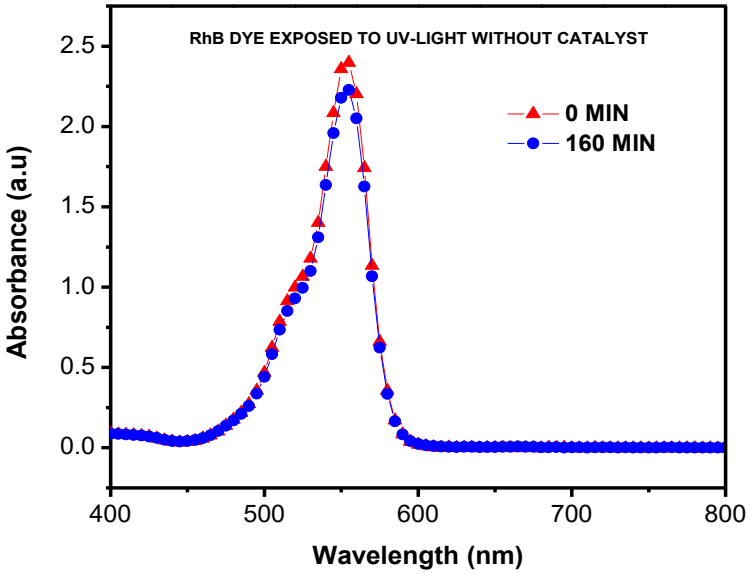

Figure 4.13: Rhodamine B without catalyst under UV light irradiation.

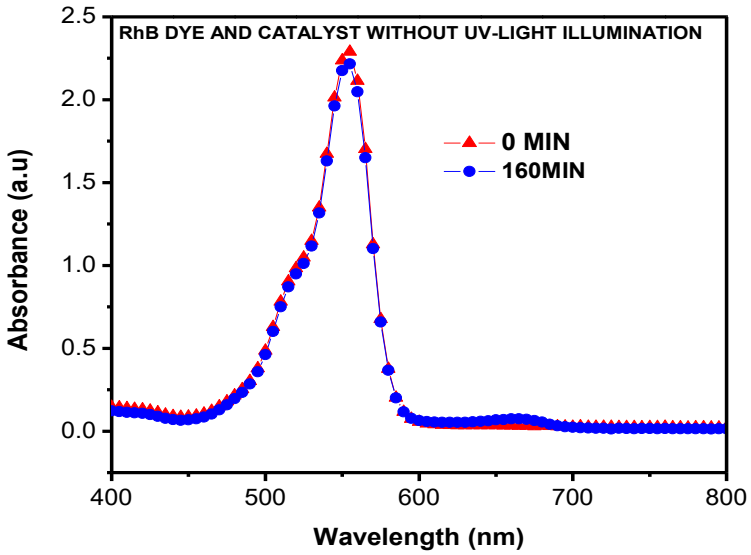

Figure 4.14: Rhodamine B with catalyst but no UV light illumination.

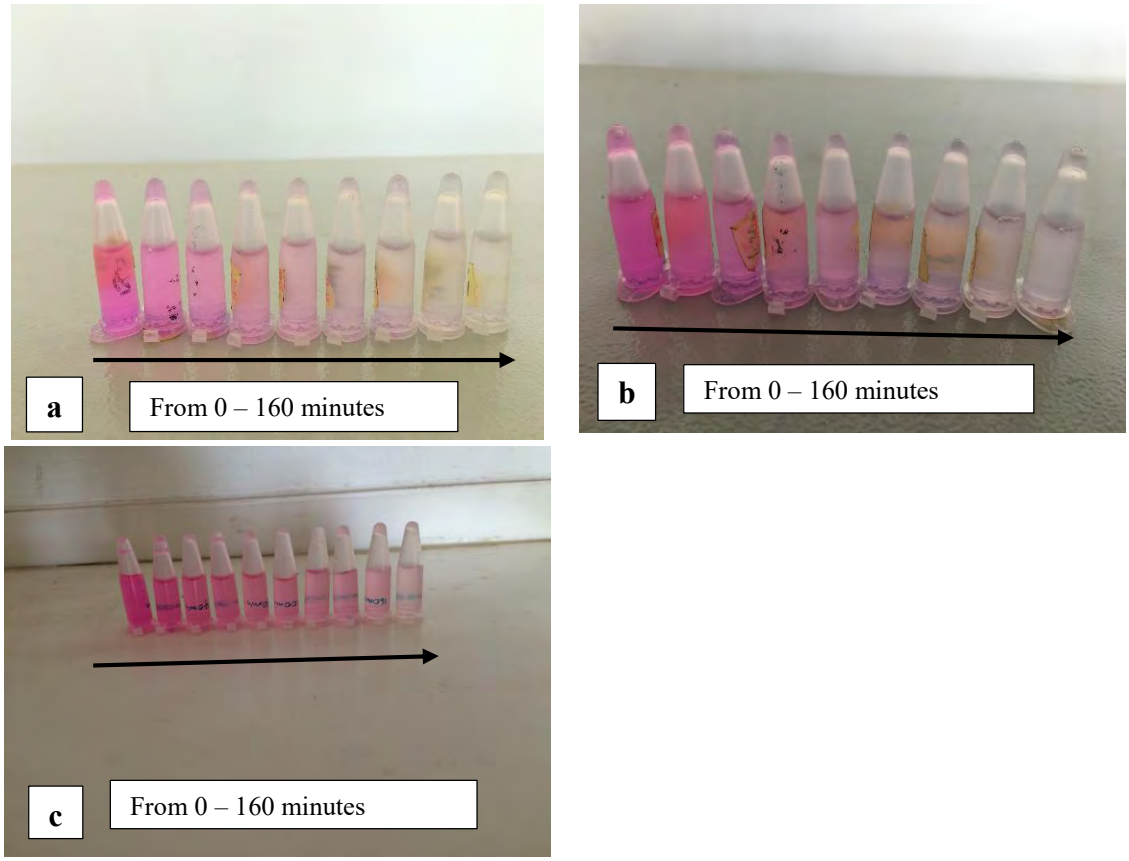

Figure 4.15: Decolourization of Rhodamine B using ZnO particles calcined at (a) 400 ℃ *(b) 500* ℃ *and (c) 600* ℃.

4.6.2 Photodegradation of Methylene Blue.

The photodegradation of Methylene blue was also carried out using ZnO nanoparticles calcined at different temperatures and a UV light source for 160 minutes. It was also observed that photodegradation of Methylene blue resulted in a decrease in the initial concentration of the dye and the decolourization of the dye after being exposed to UV light in the presence of ZnO nanoparticles for 160 minutes. Two control experiments were also conducted to investigate the factors necessary for photodegradation to occur. By this, 100 ml of Methylene blue dye without catalyst was exposed to UV light for 160 minutes. At the end of 160 minutes of irradiation, significant degradation was not observed. Also, in the second experiment, 100 ml of the dye

containing 100 mg of the catalyst was placed in a dark room for 160 minutes without UV irradiation. It was also observed that no significant degradation took place at the end of the experiment. This is an indication that both catalyst and UV light are necessary for degradation to occur. The photodegradation of Methylene Blue using ZnO nanoparticles calcined at different temperature are shown in Figures (4.16, 4.17 and 4.18). From the graphs is shown that degradation using ZnO nanoparticles calcined at 400 ℃ was the most effective as depicted in the level of absorbance at the end of 160 minutes.

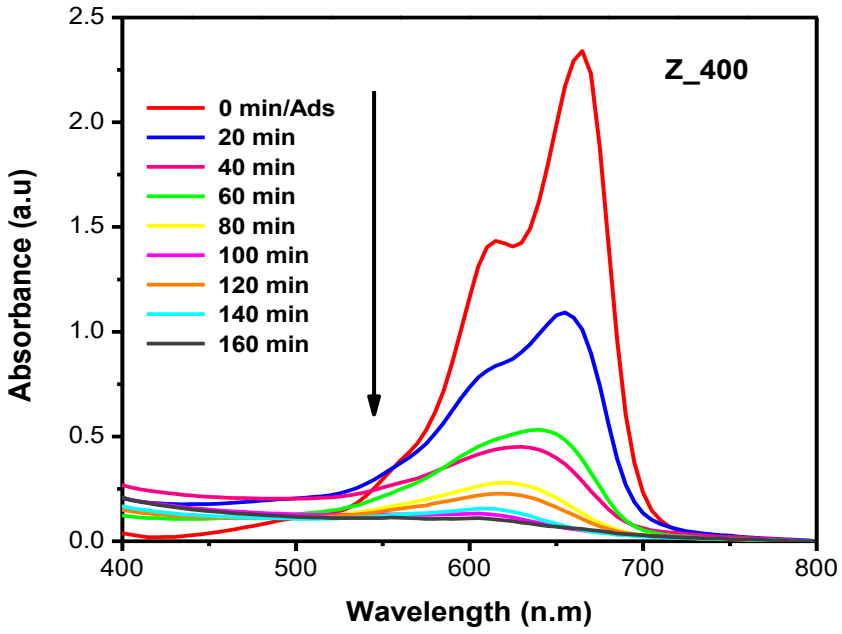

Figure 4.16: Photodegradation of MB using Z_400

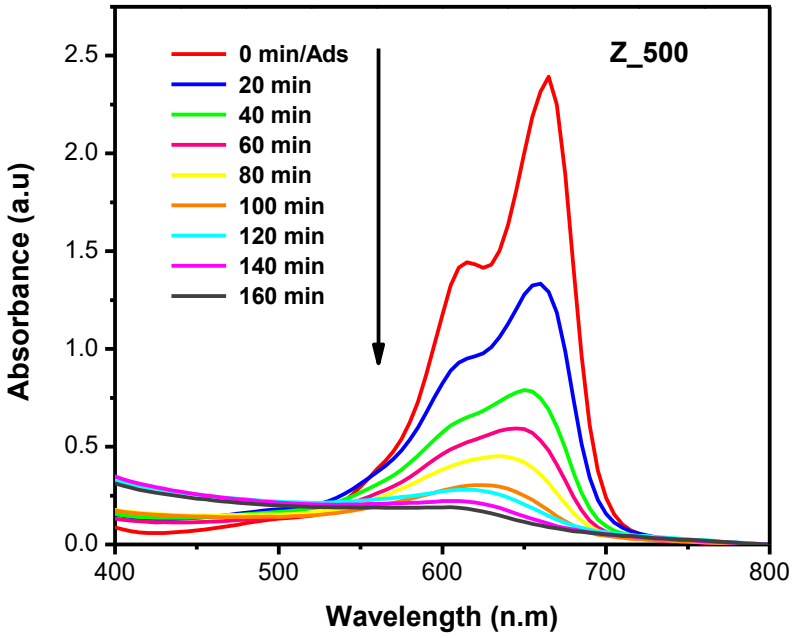

Figure 4.17: Photodegradation of MB using Z_500

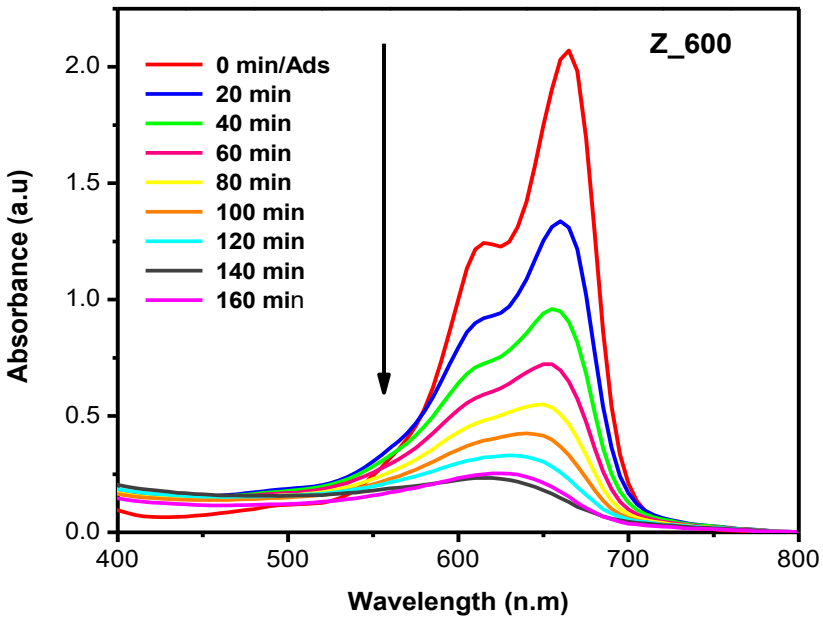

Figure 4.18: Photodegradation of MB using Z_600.

Figures 4.19 and 4.20 below also depict the degradation of the Methylene Blue dye without catalyst and Methylene Blue dye containing catalyst without UV light irradiation respectively. No significant degradation was also observed at the end of 160 minutes.

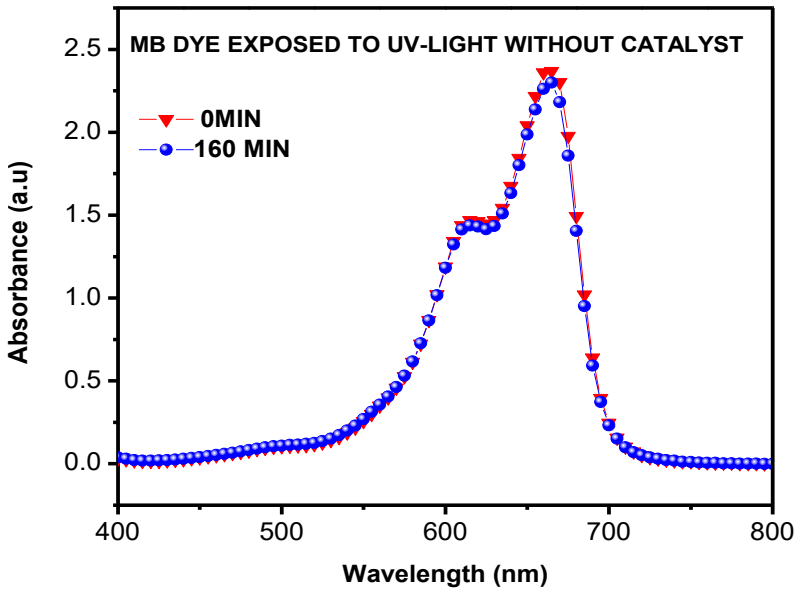

Figure 4.19: Methylene Blue without catalyst under UV light irradiation

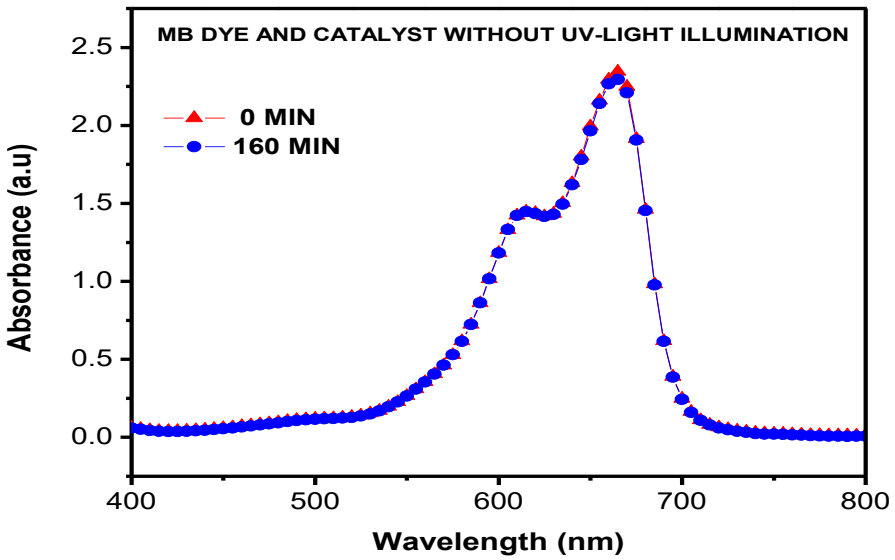

Figure 4.20: Methylene Blue with catalyst but no UV light illumination.

Decolourization of Methylene Blue after degradation is shown below (Figure 4.21).

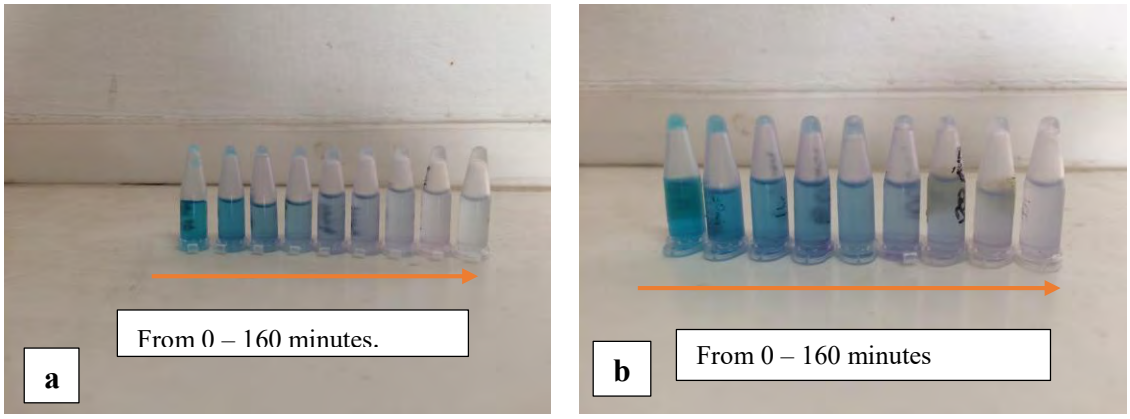

Figure 4.21: Decolourization of Methylene Blue using ZnO particles calcined at (a) 400 ℃ *(b) 500* ℃ *and (c) 600* ℃.

4.6.3 Effects of Crystallite Size on Photodegradation.

ZnO nanoparticles of different particle sizes were obtained as a result of different calcination temperatures. The particle size of ZnO nanoparticles increased with increasing temperature because larger grains were formed at higher temperatures. The effect of particle size on the photodegradation of Rhodamine B and Methylene Blue was investigated accordingly by comparing the amount of dye degraded and the amount of dye remaining after each photodegradation experiment using zinc oxide nanoparticle calcined at 400 ℃, 500 ℃, and 600 ℃. Zinc oxide nanoparticles calcined at 400 ℃ had the highest degradation effect on both dyes. The amount of dye degraded % $= \frac{C_O - C_t}{C_o} \times 100$ where C_O is the initial concentration of dye and C_t is the concentration of the dye at a particular irradiation time.

4.6.3.1 Effect of Crystallite Size on Photodegradation of Rhodamine B.

A graph of the amount of dye degraded against time and the amount of dye remaining against time are shown in **Figures 4.22** (next page). It is observed in **Figure 4.22** that the

amount of dye (RhB) degraded was highest using ZnO nanoparticles calcined at 400 ℃ followed by nanoparticles calcined at 500 ℃ and 600 ℃ respectively. This is because more active sites are provided by particles of smaller sizes to undertake photocatalytic reactions in the degradation process. Conversely, the amount of dye remaining at 160 minutes is smallest for ZnO particles calcined at 400 ℃ followed by nanoparticles calcined at 500 ℃ and 600 ℃ respectively as indicated in Table 4.2.

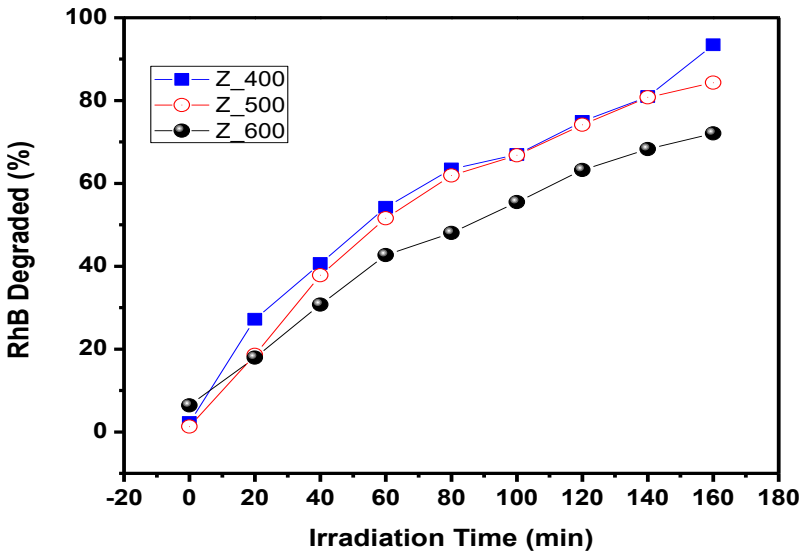

Figure 4.22: Amount of RhB degraded against time.

The effect of particle size on the degradation of Rhodamine B is summarized in table 4.2 below.

Table 4.2: Effect of crystallite size on Rhodamine B degradation.

Sample Name	Crystallite Size (nm)	Amount of Catalyst (g)	Initial Concentration of Rhodamine B (mg/l)	Final Concentration of Rhodamine B (mg/l)	Rhodamine B Degraded (%)	Rhodamine B Remaining (%)
Z_400	16	0.1	10.0	0.65	93.5	6.50
Z_500	28	0.1	10.0	1.57	84.3	15.70
Z_600	30	0.1	10.0	2.79	72.1	27.91

4.6.3.2. Effect of Crystallite Size on Photodegradation of Methylene Blue.

A graph of the amount of dye degraded against time and the amount of dye remaining against time are shown in **Figures 4.23**. It is observed in Figure **4.23** that the amount of dye (MB) degraded was highest using ZnO nanoparticles calcined at 400 ℃ followed by nanoparticles calcined at 500 ℃ and 600 ℃ respectively. This is because more active sites are provided by particles of smaller sizes to undertake photocatalytic reactions in the degradation process. Also the amount of MB dye remaining at 160 minutes is smallest for ZnO particles calcined at 400 ℃ followed by nanoparticles calcined at 500 ℃ and 600 ℃ respectively as shown in Table 4.3 (next page).

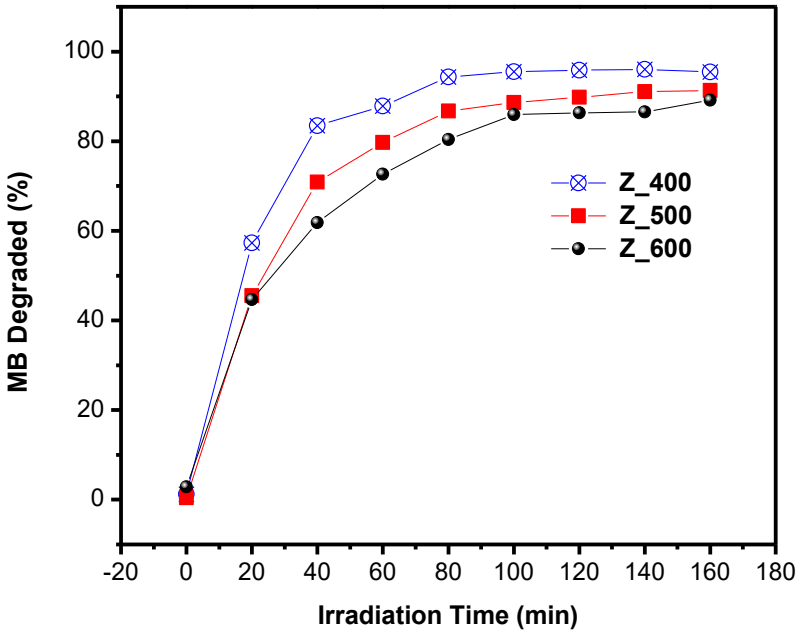

Figure 4.23: Amount MB degraded at different irradiation time

The effect of crystallite size on the photodegradation of Methylene Blue is summarized in the table below.

Table 4.3: Effect of crystallite size on MB degradation.

Sample Name	Crystallite Size (nm)	Amount Of Catalyst (g)	Initial Concentration of Methylene Blue (mg/l)	Final Concentration of Methylene Blue (mg/l)	Methylene Blue Degraded (%)	Methylene Blue Remaining (%)
Z_400	16	0.1	10.0	0.45	95.43	4.57
Z_500	28	0.1	10.0	0.87	91.34	8.66
Z_600	30	0.1	10.0	1.10	89.13	10.87

The degradation rate of Methylene Blue is higher than that of Rhodamine B for Z_400, Z_500 and Z_600 as seen in Tables 4.2 and 4.3. This can be due to pH differentials, since these dyes have different degradation rates at different pH.

4.6.4 Effect of Catalyst Load on Photodegradation.

The amount of catalyst used in the photodegradation process was varied from 0.1 g to 0.3 g with an increment of 0.05 g to determine its effect on the degradation of Rhodamine B and Methylene Blue. For every catalyst load, the volume of dye was maintained at 100 ml. Zinc oxide nanoparticles calcined at 400 ℃ were used in this experiment. A graph of the amount of Methylene Blue and Rhodamine B remaining to the time of irradiation is shown in Figure 4.24 and 4.25 respectively for the various catalyst load. It was observed for both dyes that photodegradation increased as catalyst load was increased from 0.1 g to 0.2 g and eventually decreased for 0.25 g and 0.3 g catalyst load. Catalyst load of 0.3 g recorded that lowest degradation of both dyes in 160 minutes as it comes with the highest amount of dye remaining as shown in **Figures 4.24 and 4.25** whereas the highest photodegradation was observed for 0.2 g catalyst load as it shows the lowest amount of dye remaining in 160 minutes for both dyes **in Figures 4.24 and 4.25**. This makes the 0.2 g catalyst load the optimum amount for the degradation of the dyes.

The increase in catalyst load from 0.1 g to 0.2 g, increased the number of ZnO active sites resulting in the absorption of more light photons and high adsorption of dye molecules and hence an increase in the rate of photocatalytic reaction to degrade the dyes. However, a decrease in the photodegradation of the dyes was observed as the catalyst load increased from 0.25 g to 0.3 g due to the presence of excess ZnO nanoparticles which inhibited the penetration of light and hence reduced the amount of photons absorbed. This observation may also be due to the setup used for

the photocatalytic experiment as shown in Figure 3.5 since dye – catalyst solution could not be stirred continuously throughout the experiment and this might have resulted in low light penetration for catalyst load above 0.2 g.

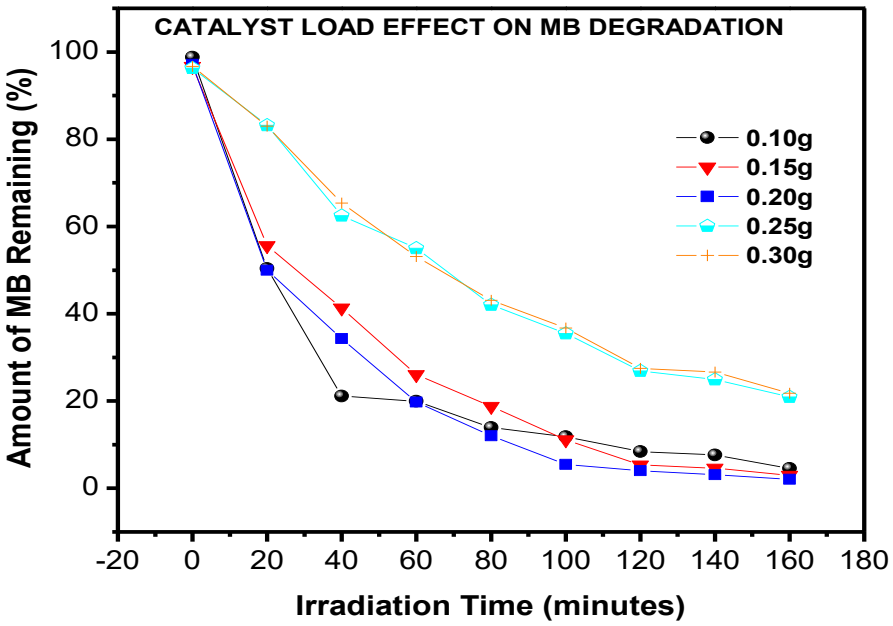

Figure 4.24: Catalyst load effect on MB Degradation.

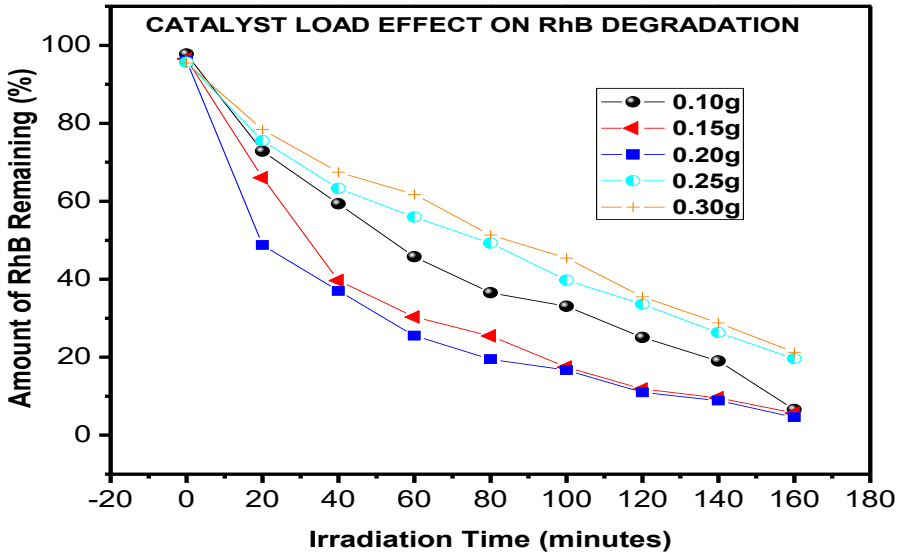

Figure 4.25: Catalyst load effect on RhB Degradation

The effect of catalyst load on the amount of dye degraded and its concentration is captured in the table blow.

Table 4.4: Effect of Catalyst Load on Dye Degradation.

Catalyst Load (g)	Initial Concentration of Rhodamine B (mg/l)	Initial Concentration of Methylene Blue (mg/l)	Final Concentration of Rhodamine B (mg/l)	Final Concentration of Methylene Blue (mg/l)	Amount of RhB Degraded (%)	Amount of MB Degraded (%)
0.10	10	10	0.65	0.45	93.45	95.43
0.15	10	10	0.56	0.29	94.37	97.04
0.20	10	10	0.46	0.20	95.41	97.97
0.25	10	10	1.97	2.08	80.35	79.10
0.30	10	10	2.13	2.18	78.72	78.21

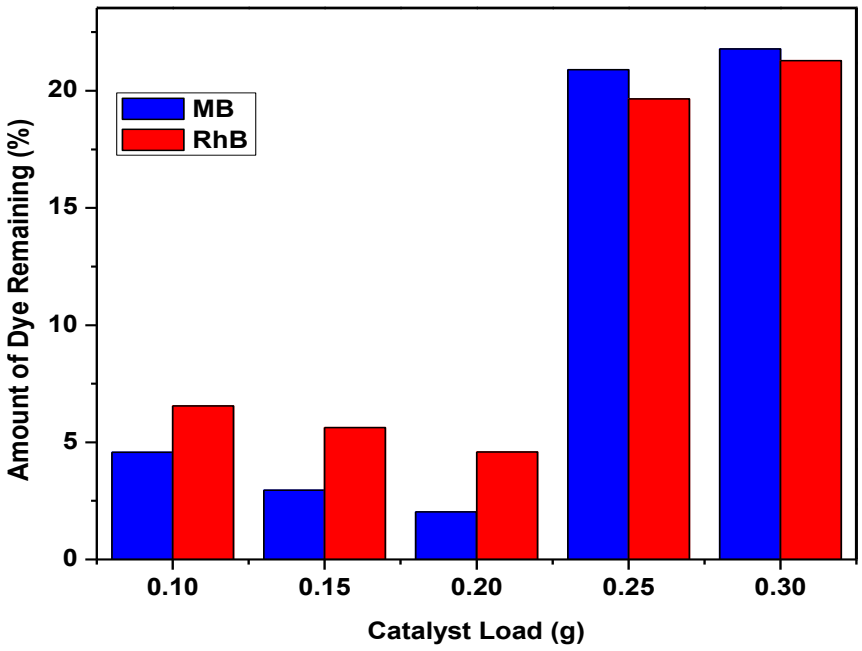

Figure 4.28: Amount of dye remaining for different catalyst load.

Amount of dye remaining decreased from 0.10 g catalyst load to 0.20 g and increased significantly for 0.25 g and 0.30 g indicating lower degradation of dyes for 0.25 g and 0.30 g catalyst load.

4.6.5 Reusability of Zinc Oxide Nanoparticles.

The tendency of zinc oxide nanoparticles to be recycled or reused for photodegradation was explored. 0.2 g of ZnO nanoparticles calcined at 400 ℃ was used to perform four cycles of degradation of Rhodamine B and Methylene Blue separately. The same particles were used for all four cycles. The particles were centrifuged, washed with distilled water and allowed to dry before being used for the next cycle. For each cycle a fresh dye solution was used. The degradation efficiency of ZnO particles for each cycle is shown in **Figure 4.29.**

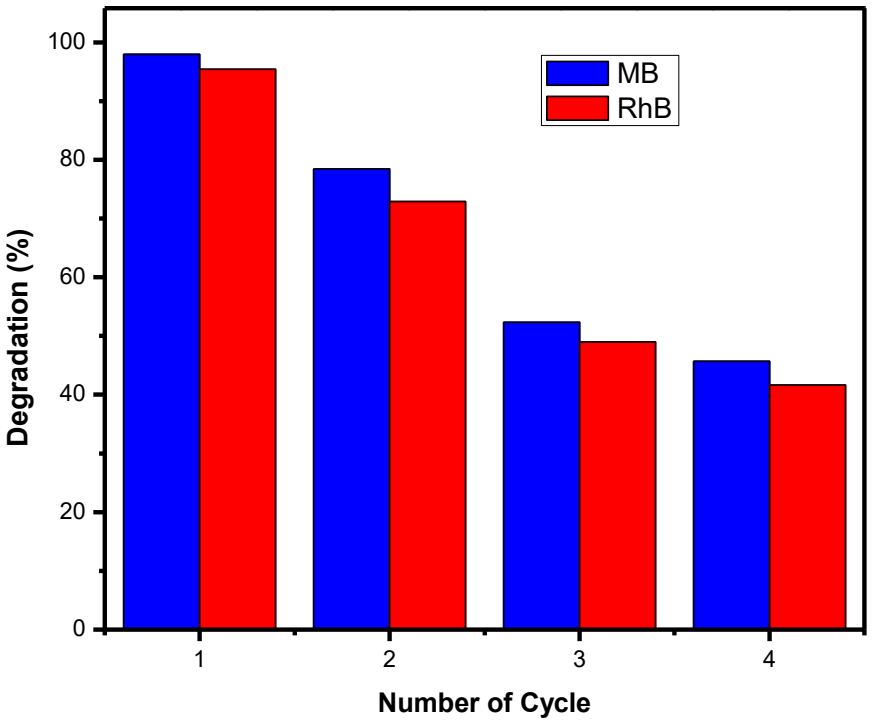

Figure 4.29: Reuse of zinc oxide nanoparticles.

A decreasing order of photodegradation efficiency of zinc oxide nanoparticles was observed from cycle 1 to cycle 4 respectively. For Methylene Blue, the degradation efficiencies were 97.97%, 78.41%, 52.3%, and 45.67% for cycles 1, 2, 3 and 4 respectively. For Rhodamine B, the degradation efficiencies were 95.41%, 72.89%, 48.95%, and 41.67% for cycles 1, 2, 3 and 4 respectively. This is attributed to the photocorrosion of zinc oxide nanoparticles [79].

CHAPTER FIVE

5.0 Conclusions and Recommendations.

Zinc oxide nanoparticles were synthesized using the sol-gel method. Three different samples were obtained by calcining the particles at different temperatures (i.e. 400 ℃, 500 ℃ and 600 ℃) and were characterized using XRD, FTIR, SEM and UV-vis spectrometry.

The XRD results analyzed for all the three samples showed a wurtzite crystal structure with characteristic distinct peaks at 31.81°, 34.44°, 36.31°, 47.602°, 56.62°, 63.01°, 66.48°, 67.97°, and 69.19° respectively. The peaks were also characteristic of crystalline zinc oxide nanoparticles. Estimation of crystallite size of nanoparticles from XRD results using the Scherer's equation showed 16 nm, 28 nm and 30 nm for zinc oxide nanoparticles calcined at 400 ℃, 500 ℃ and 600 ℃ respectively. This indicates that particle size increases with increasing calcination temperature.

FTIR spectra of all the three samples confirmed the presence of Zn – O bond vibrations and Zn metal with characteristic bands showing at 861 cm^{-1} and 688 cm^{-1} respectively. Broad bands between 3400 cm^{-1} and 3500 cm^{-1} were also associated with hydroxyl groups owing to water molecules adsorbed onto zinc oxide nanoparticles.

UV-vis analysis revealed that the absorption spectrum of all three samples lie in the ultraviolet region of the electromagnetic spectrum with absorption wavelength ranging from 370 nm to 375 nm. Band gap energy estimated from Tauc plot showed 3.2 eV, 3.1 eV and 3.0 eV for ZnO nanoparticles calcined at 400 ℃, 500 ℃ and 600 ℃ respectively. A decrease in bandgap energy as the temperature was increased was observed and this phenomenon is usually identified with semiconductor materials due to quantum confinement effect.

SEM images of zinc oxide nanoparticles also showed rice-like morphology. The images also showed that particle agglomeration occurred at all temperatures in an increasing order from 400 ℃ to 600 ℃ as a result of grain growth.

The zinc oxide nanoparticles were also used in a photocatalytic experiment to degrade Rhodamine B and Methylene Blue in the presence of UV – light. Photodegradation did not significantly occur in the absence of either light or catalyst and this shows that both are needed for photodegradation to occur. Degradation efficiency however decreased for ZnO nanoparticles calcined at 400 ℃, 500 ℃ and 600 ℃ respectively due increase in particle size resulting into low surface area. For Rhodamine B dye, the initial concentration of 10 mg/l decreased to 0.65 mg/l, 1.57 mg/l and 2.79 mg/l representing 93.5%, 84.3% and 72.1% of degradation when zinc oxide nanoparticles calcined at 400 ℃, 500 ℃ and 600 ℃ were used respectively. For Methylene Blue, the initial concentration of 10 mg/l decreased to 0.45 mg/l, 0.87 mg/l and 1.10 mg/l representing 95.4 %, 91.3 % and 89.1 % of degradation when zinc oxide nanoparticles calcined at 400 ℃, 500 ℃ and 600 ℃ respectively were used. Therefore the optimum calcination temperature is 400 ℃.

Catalyst load was varied using 0.10 g, 0.15 g, 0.20 g, 0.25 g and 0.30 g to investigate their effect on degradation efficiency. The highest degradation was recorded when 0.20 g of zinc oxide was used whereas the lowest degradation was recorded for 0.30 g catalyst load. In effect, the optimum catalyst load was 0.2 g with 95.41 % and 97.97 % degradation of Rhodamine B and Methylene Blue respectively in 160 minutes. In general, final concentration of dyes decreased when the catalyst amount was increased from 0.1 g to 0.2 g indicating an increase in the degradation whiles a decrease in the degradation was observed when the catalyst amount was increased to 0.25 g and 0.3 g. The decrease in degradation may be due to high catalyst density and low light penetration.

Reusability of zinc oxide nanoparticles was determined by measuring the degradation efficiency of the same catalyst used in four different cycles of degradation. Degradation of dyes occurred in all four cycles in a decreasing order due to photocorrosion of ZnO nanoparticles.

Doping of ZnO with metallic and non-metallic elements to can be explored to increase its range of absorption into the visible light spectrum. Also ZnO thin films for photocatalysis is also recommended for easy recovery after use.

References

[1] E. A. El-Sharkawy, A. Y. Soliman, and K. M. Al-Amer, "Comparative study for the removal of methylene blue via adsorption and photocatalytic degradation," *J. Colloid Interface Sci.*, vol. 310, no. 2, pp. 498–508, 2007.

[2] V. Jadhav, P. Chikode, G. Nikam, and S. Sabale, "Polyol synthesis and characterization of ZnO@CoFe2O4 MNP's to study the photodegradation rate of azo and diphenyl type dye," *Mater. Today Proc.*, vol. 3, no. 10, pp. 4121–4127, 2016.

[3] R. Saleh and N. F. Djaja, "UV light photocatalytic degradation of organic dyes with Fe-doped ZnO nanoparticles," *Superlattices Microstruct.*, vol. 74, pp. 217–233, 2014.

[4] A. Balcha, O. P. Yadav, and T. Dey, "Photocatalytic degradation of methylene blue dye by zinc oxide nanoparticles obtained from precipitation and sol-gel methods," *Environ. Sci. Pollut. Res.*, 2016.

[5] M. Blue, B. G. Ankamwar, V. B. Kamble, J. I. Annsi, L. S. Sarma, and C. M. Mahajan, "Solar Photocatalytic Degradation of," vol. 17, no. 2, 2017.

[6] H. Zollinger, "Color: A multidisciplinary approach," *Color A Multidiscip. Approach*, pp. 1–258, 2006.

[7] S. S. Vieira, Z. M. Magriotis, N. A. V Santos, M. das G. Cardoso, and A. A. Saczk, "Macauba palm (Acrocomia aculeata) cake from biodiesel processing: An efficient and low cost substrate for the adsorption of dyes," *Chem. Eng. J.*, vol. 183, pp. 152–161, 2012.

[8] H. X. Guo, K. L. Lin, Z. S. Zheng, F. Bin Xiao, and S. X. Li, "Sulfanilic acid-modified P25 TiO2nanoparticles with improved photocatalytic degradation on Congo red under visible light," *Dye. Pigment.*, vol. 92, no. 3, pp. 1278–1284, 2012.

[9] H. Kyung, J. Lee, and W. Choi, "Simultaneous and synergistic conversion of dyes and heavy metal ions in aqueous TiO2 suspensions under visible-light illumination," *Environ. Sci. Technol.*, vol. 39, no. 7, pp. 2376–2382, 2005.

[10] M. R. Hoffmann, S. T. Martin, W. Choi, and D. W. Bahnemann, "Environmental Applications of Semiconductor Photocatalysis," *Chem. Rev.*, vol. 95, no. 1, pp. 69–96,

1995.

[11] C. B. Ong, L. Y. Ng, and A. W. Mohammad, "A review of ZnO nanoparticles as solar photocatalysts: Synthesis, mechanisms and applications," *Renew. Sustain. Energy Rev.*, vol. 81, no. July 2016, pp. 536–551, 2018.

[12] R. Ameta, M. S. Solanki, S. Benjamin, and S. C. Ameta, *Photocatalysis*. 2018.

[13] S. Gardin *et al.*, "Photocatalytic Performance of Hybrid SiO 2 −TiO 2 Films," *J. Phys. Chem. C*, vol. 114, no. 17, pp. 7646–7652, 2010.

[14] L. Chen *et al.*, "Preparation of TiO2nanofilm via sol-gel process and its photocatalytic activity for degradation of methyl orange," *Ceram. Int.*, vol. 35, no. 8, pp. 3275–3280, 2009.

[15] A. nan Wang *et al.*, "Diphenylarsinic acid contaminated soil remediation by titanium dioxide (P25) photocatalysis: Degradation pathway, optimization of operating parameters and effects of soil properties," *Sci. Total Environ.*, vol. 541, pp. 348–355, 2016.

[16] S. M. Lam, J. C. Sin, A. Z. Abdullah, and A. R. Mohamed, "Degradation of wastewaters containing organic dyes photocatalysed by zinc oxide: A review," *Desalin. Water Treat.*, vol. 41, no. 1–3, pp. 131–169, 2012.

[17] E. R. Carraway, A. J. Hoffman, and M. R. Hoffmann, "Photocatalytic Oxidation of Organic-Acids on Quantum-Sized Semiconductor Colloids," *Environ. Sci. Technol.*, vol. 28, no. 5, pp. 786–793, 1994.

[18] S. Baruah, M. Jaisai, R. Imani, M. M. Nazhad, and J. Dutta, "Photocatalytic paper using zinc oxide nanorods," *Sci. Technol. Adv. Mater.*, vol. 11, no. 5, 2010.

[19] X. Zhang *et al.*, "Carbon-Doped ZnO Nanostructures: Facile Synthesis and Visible Light Photocatalytic Applications," *J. Phys. Chem. C*, vol. 119, no. 35, pp. 20544–20554, 2015.

[20] S. Majumdar and P. Banerji, "Moisture sensitivity of p-ZnO/n-Si heterostructure," *Sensors Actuators, B Chem.*, vol. 140, no. 1, pp. 134–138, 2009.

[21] A. Kolodziejczak-Radzimska and T. Jesionowski, "Zinc oxide-from synthesis to application: A review," *Materials (Basel).*, vol. 7, no. 4, pp. 2833–2881, 2014.

[22] Y. T. Chung, M. M. Ba-Abbad, A. W. Mohammad, N. H. H. Hairom, and A. Benamor, "Synthesis of minimal-size ZnO nanoparticles through sol-gel method: Taguchi design optimisation," *Mater. Des.*, vol. 87, pp. 780–787, 2015.

[23] A. C. Mohan and B. Renjanadevi, "Preparation of Zinc Oxide Nanoparticles and its Characterization Using Scanning Electron Microscopy (SEM) and X-Ray Diffraction(XRD)," *Procedia Technol.*, vol. 24, pp. 761–766, 2016.

[24] S. Suresh, "Semiconductor Nanomaterials, Methods and Applications: A Review," *Nanosci. Nanotechnol.*, vol. 3, no. 3, pp. 62–74, 2013.

[25] V. K. Vidhu and D. Philip, "Catalytic degradation of organic dyes using biosynthesized silver nanoparticles," *Micron*, vol. 56, pp. 54–62, 2014.

[26] A. P. Alivisatos, "Perspectives on the physical chemistry of semiconductor nanocrystals," *J. Phys. Chem.*, vol. 100, no. 31, pp. 13226–13239, 1996.

[27] A. J. Meaney, "On The Growth and Characterisation of Zinc Oxide," p. 105, 2010.

[28] P. Uikey and K. Vishwakarma, "Review OF Zinc oxide (ZNO) Nanoparticles applications and Properties," *Int. J. Emerg. Technol. Comput. Sci. Electron.*, vol. 21, no. 2, pp. 976–1353, 2016.

[29] Y. Zhang, M. K. Ram, E. K. Stefanakos, and D. Y. Goswami, "Synthesis, characterization, and applications of ZnO nanowires," *J. Nanomater.*, vol. 2012, 2012.

[30] Y. Sun *et al.*, "The Applications of Morphology Controlled ZnO in Catalysis," *Catalysts*, vol. 6, no. 12, p. 188, 2016.

[31] M. Ozgür, D. Hofstetter, and H. Morkoç, "ZnO Devices and Applications: A Review of Current Status and Future Prospects," *Proc. IEEE*, vol. 98, pp. 1255–1268, 2010.

[32] S. Tammas-Williams and I. Todd, "Design for additive manufacturing with site-specific properties in metals and alloys," *Scr. Mater.*, vol. 135, pp. 105–110, 2017.

[33] A. Ashrafi and C. Jagadish, "Review of zincblende ZnO: Stability of metastable ZnO phases," *J. Appl. Phys.*, vol. 102, no. 7, 2007.

[34] A. Kumar, N. Yadav, M. Bhatt, N. K. Mishra, P. Chaudhary, and R. Singh, "Sol-Gel

Derived Nanomaterials and It ' s Applications : A Review," *Res. J. Chem. Sci.*, vol. 5, no. 12, pp. 98–105, 2015.

[35] P. Tonto, O. Mekasuwandumrong, S. Phatanasri, V. Pavarajarn, and P. Praserthdam, "Preparation of ZnO nanorod by solvothermal reaction of zinc acetate in various alcohols," *Ceram. Int.*, vol. 34, no. 1, pp. 57–62, 2008.

[36] P. G. McCormick and F. H. Froes, "The fundamentals of mechanochemical processing," *Jom*, vol. 50, no. 11, pp. 61–65, 1998.

[37] L. L. Hench and J. K. West, "The Sol-Gel Process," *Chem. Rev.*, vol. 90, no. 1, pp. 33–72, 1990.

[38] H. Benhebal *et al.*, "Photocatalytic degradation of phenol and benzoic acid using zinc oxide powders prepared by the sol-gel process," *Alexandria Eng. J.*, vol. 52, no. 3, pp. 517–523, 2013.

[39] A. B. Djurišić, X. Y. Chen, and Y. H. Leung, "Recent progress in hydrothermal synthesis of zinc oxide nanomaterials," *Recent Pat. Nanotechnol.*, vol. 6, no. 2, pp. 124–134, 2012.

[40] L. N. Dem'yanets, L. E. Li, and T. G. Uvarova, "Zinc oxide: Hydrothermal growth of nano- and bulk crystals and their luminescent properties," *J. Mater. Sci.*, vol. 41, no. 5, pp. 1439–1444, 2006.

[41] G. Demazeau, "Solvothermal processes-A route to the stabilization of new materials," *J Mater Chem*, vol. 9, no. 1, pp. 15–18, 1999.

[42] M. Rajamathi and R. Seshadri, "Oxide and chalcogenide nanoparticles from hydrothermal/solvothermal reactions," *Curr. Opin. Solid State Mater. Sci.*, vol. 6, no. 4, pp. 337–345, 2002.

[43] T. K. Achar, A. Bose, and P. Mal, "Mechanochemical synthesis of small organic molecules," *Beilstein J. Org. Chem.*, vol. 13, pp. 1907–1931, 2017.

[44] R. B. N. Baig and R. S. Varma, "Alternative energy input: Mechanochemical, microwave and ultrasound-assisted organic synthesis," *Chem. Soc. Rev.*, vol. 41, no. 4, pp. 1559–1584, 2012.

[45] S. S. Srinivasan, J. Wade, E. K. Stefanakos, and Y. Goswami, "Synergistic effects of sulfation and co-doping on the visible light photocatalysis of TiO2," *J. Alloys Compd.*, vol. 424, no. 1–2, pp. 322–326, 2006.

[46] H. Zhang, X. Lv, Y. Li, Y. Wang, and J. Li, "P25-graphene composite as a high performance photocatalyst (Functionalized graphene)," *ACS Nano*, vol. 4, no. 1, pp. 380–386, 2010.

[47] D. Y. Goswami, "Decontamination of Ventilation Systems Using Photocatalytic Air Cleaning Technology," *J. Sol. Energy Eng.*, vol. 125, no. 3, p. 359, 2003.

[48] A. Vohra, D. Y. Goswami, D. A. Deshpande, and S. S. Block, "Enhanced photocatalytic disinfection of indoor air," *Appl. Catal. B Environ.*, vol. 64, no. 1–2, pp. 57–65, 2006.

[49] S. Baruah, M. A. Mahmood, M. T. Z. Myint, T. Bora, and J. Dutta, "Enhanced visible light photocatalysis through fast crystallization of zinc oxide nanorods," *Beilstein J. Nanotechnol.*, vol. 1, no. 1, pp. 14–20, 2010.

[50] S. Rehman, R. Ullah, A. M. Butt, and N. D. Gohar, "Strategies of making TiO2and ZnO visible light active," *J. Hazard. Mater.*, vol. 170, no. 2–3, pp. 560–569, 2009.

[51] S. Ahmed, M. G. Rasul, W. N. Martens, R. Brown, and M. A. Hashib, "Heterogeneous photocatalytic degradation of phenols in wastewater: A review on current status and developments," *Desalination*, vol. 261, no. 1–2, pp. 3–18, 2010.

[52] D. B. Ingram and S. Linic, "Photoelectrodes : Evidence for Selective Plasmon-Induced Formation," pp. 5202–5205, 2011.

[53] S. S. Srinivasan, J. Wade, and E. K. Stefanakos, "Synthesis and Characterization of Photocatalytic *J. Nanomater.*, vol. 2006, pp. 1–4, 2006.

[54] Z. Yi, X. Xu, X. Duan, W. Zhu, Z. Zhou, and X. Fan, "Photocatalytic activity and stability of ZnO particles with different morphologies," *Rare Met.*, vol. 30, no. SUPPL.1, pp. 183–187, 2011.

[55] K. Pirkanniemi and M. Sillanpää, "Heterogeneous water phase catalysis as an environmental application: A review," *Chemosphere*, vol. 48, no. 10, pp. 1047–1060,

2002.

[56] J. P. Percherancier, R. Chapelon, and B. Pouyet, “Semiconductor-sensitized photodegradation of pesticides in water: the case of carbetamide,” *J. Photochem. Photobiol. A Chem.*, vol. 87, no. 3, pp. 261–266, 1995.

[57] N. Daneshvar, D. Salari, and A. R. Khataee, “Photocatalytic degradation of azo dye acid red 14 in water on ZnO as an alternative catalyst to TiO2,” *J. Photochem. Photobiol. A Chem.*, vol. 162, no. 2–3, pp. 317–322, 2004.

[58] M. Klare, J. Scheen, K. Vogelsang, H. Jacobs, and J. A. C. Broekaert, “Degradation of short-chain alkyl- and alkanolamines by TiO2- and Pt/TiO2-assisted photocatalysis,” *Chemosphere*, vol. 41, no. 3, pp. 353–362, 2000.

[59] C. B. Ong, L. Y. Ng, and A. W. Mohammad, “A review of ZnO nanoparticles as solar photocatalysts: Synthesis, mechanisms and applications,” *Renew. Sustain. Energy Rev.*, vol. 81, no. August 2017, pp. 536–551, 2018.

[60] A. Gürses, M. Açıkyıldız, K. Güneş, and M. S. Gürses, “Dyes and Pigments,” 2016.

[61] K. S. Suslick, “Sonochemistry,” *Kirk-Othmer Encyclopedia of Chemical Tecnology*. pp. 516–541, 1998.

[62] S.-Y. Pung, W.-P. Lee, and A. Aziz, “Kinetic Study of Organic Dye Degradation Using ZnO Particles with Different Morphologies as a Photocatalyst,” *Int. J. Inorg. Chem.*, vol. 2012, pp. 1–9, 2012.

[63] M. F. Al-Kadhemy, I. F. Alsharuee, and A. A. D. Al-Zuky, “Analysis of the effect of the concentration of rhodamine B in ethanol on the fluorescence spectrum using the ‘Gauss Mod’ function,” *J. Phys. Sci.*, vol. 22, no. 2, pp. 77–86, 2011.

[64] S. Merouani, O. Hamdaoui, F. Saoudi, M. Chiha, and C. Pétrier, “Influence of bicarbonate and carbonate ions on sonochemical degradation of Rhodamine B in aqueous phase,” *J. Hazard. Mater.*, vol. 175, no. 1–3, pp. 593–599, 2010.

[65] I. S. Yahia, Y. S. Rammah, and K. F. Khaled, “Fabrication of an electrochemical cell based on Rhodamine B Dye for low power applications,” *J. Mater. Environ. Sci.*, vol. 4,

no. 3, 2013.

[66] L. M. Moreira, J. P. Lyon, A. P. Romani, D. Severino, M. R. Rodrigues, and H. P. M. de Oliveira, "Phenotiazinium Dyes as Photosensitizers (PS) in Photodynamic Therapy (PDT): Spectroscopic Properties and Photochemical Mechanisms," *Adv. Asp. Spectrosc.*, pp. 393–422, 2012.

[67] F. Harris and L. Pierpoint, "PhotodynamicTherapy Based on 5-Aminolevulinic Acid and Its Use as an Antimicrobial Agent," *Med. Res. Rev.*, vol. 29, no. 6, pp. 1292–1327, 2012.

[68] X. Chen, Z. Wu, D. Liu, and Z. Gao, "Preparation of ZnO Photocatalyst for the Efficient and Rapid Photocatalytic Degradation of Azo Dyes," *Nanoscale Res. Lett.*, vol. 12, no. 1, pp. 4–13, 2017.

[69] P. Application, "University of Ghana http://ugspace.ug.edu.gh NANOSTRUCTURED TITANIUM DIOXIDE : SYNTHESIS , CHARACTERIZATION AND PHOTOACTIVE APPLICATION BY," no. 10278265, 2016.

[70] P. Magalh, L. Andrade, O. C. Nunes, and A. Mendes, "TITANIUM DIOXIDE PHOTOCATALYSIS : FUNDAMENTALS AND APPLICATION ON PHOTOINACTIVATION," 2017.

[71] M. A. Lazar, S. Varghese, and S. S. Nair, "Photocatalytic Water Treatment by Titanium Dioxide: Recent Updates," pp. 572–601, 2012.

[72] D. R. Shinde, P. S. Tambade, M. G. Chaskar, and K. M. Gadave, "Photocatalytic degradation of dyes in water by analytical reagent grades ZnO , TiO 2 and SnO 2 : a comparative study," pp. 109–117, 2017.

[73] M. W. Kadi and R. M. Mohamed, "Enhanced Photocatalytic Activity of ZrO 2 -SiO 2 Nanoparticles by Platinum Doping," vol. 2013, 2013.

[74] S. N. Basahel, T. T. Ali, M. Mokhtar, and K. Narasimharao, "Influence of crystal structure of nanosized ZrO 2 on photocatalytic degradation of methyl orange," 2015.

[75] H. Kumar and R. Rani, "Structural and Optical Characterization of ZnO Nanoparticles Synthesized by Microemulsion Route," *Int. Lett. Chem. Phys. Astron.*, vol. 19, pp. 26–36,

2013.

[76] Z. R. Khan, M. S. Khan, M. Zulfequar, and M. S. Khan, "Optical and Structural Properties of ZnO Thin Films Fabricated by Sol-Gel Method," vol. 2011, no. May, pp. 340–345, 2011.

[77] A. B. Lavand and Y. S. Malghe, "Synthesis, characterization and visible light photocatalytic activity of nitrogen-doped zinc oxide nanospheres," *J. Asian Ceram. Soc.*, vol. 3, no. 3, pp. 305–310, 2015.

[78] A. K. Zak, M. E. Abrishami, W. H. A. Majid, R. Yousefi, and S. M. Hosseini, "Effects of annealing temperature on some structural and optical properties of ZnO nanoparticles prepared by a modified sol-gel combustion method," *Ceram. Int.*, vol. 37, no. 1, pp. 393–398, 2011.

[79] S. B. A. Hamid, S. J. Teh, and C. W. Lai, "Photocatalytic Water Oxidation on ZnO: A Review," *Catalysts*, vol. 7, no. 3, p. 93, 2017.